

AN ABSTRACT OF THE THESIS OF

Charles Hartgraves Black for the Ph. D. in Mechanical Engineering
(Name) (Degree) (Major)

Date thesis is presented Oct. 7, 1966

Title EFFECTIVENESS OF A FLUIDIZED BED IN FILTRATION OF
AIRBORNE PARTICULATE OF SUBMICRON SIZE

Abstract approved [REDACTED]
(Major professor)

Submicron particulate (mean size of 0.52 microns) was filtered from air at substantially atmospheric temperature and pressure by passing air up through a bed of fluidized glass shot in a two inch column. Removal efficiency, defined as the percentage removal of particulate from the air stream, was essentially constant during the life of the bed and independent of the entering concentration over the range of 0.1 to 5 milligrams per cubic meter. Varying superficial gas flow rates from 8.75 to 25 feet per minute and bed heights from 5 to 12 inches, resulted in filtration efficiencies ranging from about 50 to 90 percent. Removal efficiency of the fluidized bed improved with increased bed height and decreasing superficial gas flow velocities.

Analysis of filtration mechanisms indicated that inertial impaction forces may be considered negligible and that the predominant effects are Brownian diffusion, direct interception and induced electrostatic attraction. An equation is presented describing effective

filtration efficiency as a function of mean sizes of challenging aerosol and bed material, air viscosity and density, bed height-to-diameter ratio, and superficial gas flow velocity.

Analyses and tests indicated particulate approximately 0.5 micron in diameter to be the most difficult to remove from the air stream by use of the fluidized bed. Filtration efficiencies were found for both larger and smaller particles.

EFFECTIVENESS OF A FLUIDIZED BED IN FILTRATION
OF AIRBORNE PARTICULATE OF SUBMICRON SIZE

by

CHARLES HARTGRAVES BLACK

A THESIS

submitted to

OREGON STATE UNIVERSITY

in partial fulfillment of
the requirements for the
degree of

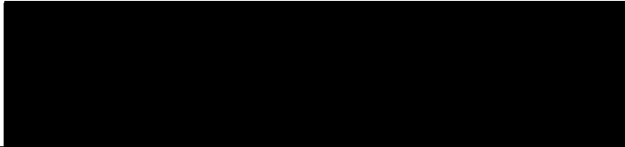
DOCTOR OF PHILOSOPHY

June 1967


APPROVED:



Associate Professor of Mechanical Engineering
In Charge of Major



Head of Department of Mechanical Engineering



Dean of Graduate School

Date thesis is presented Oct. 7, 1966

Typed by Donna Olson

ACKNOWLEDGEMENTS

The author gratefully acknowledges the Public Health Service for supporting the research through Division of Air Pollution Grant 5F3 AP23, 925.

TABLE OF CONTENTS

	<u>Page</u>
INTRODUCTION	1
The Problem	1
The Selected Bed Geometry	2
LITERATURE REVIEW	3
Fluidized Beds as Adsorption Media	3
Filtration Mechanisms	4
Interception	5
Inertial Impaction	7
Brownian Diffusion	9
Electrostatic Attraction	10
Generalizations	11
FLUIDIZED BEDS	14
STIRRED SETTLING CHAMBER	19
EXPERIMENTAL PROGRAM	22
Scope	22
Experimental Apparatus	22
Over-All Description	22
Aerosol Generator	26
Stirred Settling Chamber Assembly	26
Fluidized Bed Assembly	27
Aerosol Photometer	27
Experimental Procedures	29
RESULTS	33
CONCLUSIONS	57
BIBLIOGRAPHY	69
APPENDIX A	71
APPENDIX B	77

LIST OF FIGURES

<u>Figure</u>	<u>Page</u>
1. Streamlines and Particle Trajectories Approaching Filter Element.	6
2. Approximate Solutions of Equations for Target Efficiencies.	13
3. Pressure Drop Across Fluidized Bed vs. Superficial Gas Flow Rate.	16
4. Nomograph for use in Calculating Stokesian Radius from Half-Life Data (Chamber Height 50 cm.).	21
5. Schematic Flow Diagram.	23
6a. Apparatus for Determining Filtration Efficiencies of a Fluidized Bed, Generalized Views.	24
6b. Apparatus for Determining Filtration Efficiencies of a Fluidized Bed, Fluidizing Column and Four-way Reversing Valve.	25
7. Fluidized Bed Material Size Distribution, Logarithmic Probability Graph.	28
8. Recording Trace of Photometer Read-Out vs. Time. c_1 Indicates Reading While Sampling Challenging Aerosol; c_2 Indicates Reading While Sampling Penetrating Aerosol.	30
9. Aerosol Photometer Calibration Graph.	32
10. Percent Light Scatter vs. Time for Challenging Aerosol, c_1 and Penetrating Aerosol, c_2 . $h = 2$, $V_o = 8.75$ ft/min.	40
11. Percent Light Scatter vs. Time for Challenging Aerosol, c_1 and Penetrating Aerosol, c_2 . $h = 2$, $V_o = 10.96$ ft/min.	41
12. Percent Light Scatter vs. Time for Challenging Aerosol, c_1 and Penetrating Aerosol, c_2 . $h = 2$, $V_o = 14.65$ ft/min.	42

<u>Figure</u>	<u>Page</u>
13. Percent Light Scatter vs. Time for Challenging Aerosol, c_1 and Penetrating Aerosol, c_2 . $h = 2$, $V_o = 25.00$ ft/min.	43
14. Percent Light Scatter vs. Time for Challenging Aerosol, c_1 and Penetrating Aerosol, c_2 . $h = 4$, $V_o = 8.75$ ft/min.	44
15. Percent Light Scatter vs. Time for Challenging Aerosol, c_1 and Penetrating Aerosol, c_2 . $h = 4$, $V_o = 10.96$ ft/min.	45
16. Percent Light Scatter vs. Time for Challenging Aerosol, c_1 and Penetrating Aerosol, c_2 . $h = 4$, $V_o = 14.65$ ft/min.	46
17. Percent Light Scatter vs. Time for Challenging Aerosol, c_1 and Penetrating Aerosol, c_2 . $h = 4$, $V_o = 25.00$ ft/min.	47
18. Percent Light Scatter vs. Time for Challenging Aerosol, c_1 and Penetrating Aerosol, c_2 . $h = 6$, $V_o = 8.75$ ft/min.	48
19. Percent Light Scatter vs. Time for Challenging Aerosol, c_1 and Penetrating Aerosol, c_2 . $h = 6$, $V_o = 10.96$ ft/min.	49
20. Percent Light Scatter vs. Time for Challenging Aerosol, c_1 and Penetrating Aerosol, c_2 . $h = 6$, $V_o = 14.65$ ft/min.	50
21. Percent Light Scatter vs. Time for Challenging Aerosol, c_1 and Penetrating Aerosol, c_2 . $h = 6$, $V_o = 25.00$ ft/min.	51
22. Size Distribution of Challenging Aerosol (NH_4Cl), Logarithmic Probability Graph.	52
23. Results of Pressure Drop Measurements Across Fluidized Bed at Various Gas Flow Rates and Bed Heights.	53

<u>Figure</u>	<u>Page</u>
24. Results of Fluidized Bed Filtration Efficiency Measurements for Different Levels of Challenging Aerosol Concentration.	54
25. Recalculated Data Showing Single Valued Functions with Slope of 1.78.	55
26. Efficiency Data and Curve Representing Equation 28.	56
27a. Photomicrograph (1000X) of Bed Material before Being used as Filtration Media. Dark Ring is Part of Glass Shot out of Depth of Focusing Field.	59
27b. Photomicrograph (1000X) of Bed Material after being used as Filtration Media.	59
28. Effective Filter Efficiency vs. Particle Size for Different Flow Rates. Filtration Mechanisms are Brownian Diffusion and Interception.	63
29. Fluidized Bed Effective Filter Efficiency vs. Challenging Aerosol Particle Size for Various Bed Height-to-diameter Ratios, h.	64

LIST OF TABLES

<u>Table</u>	<u>Page</u>
I. Results of Fluidized Bed Filtration Efficiency Measurements	36
II. Filtration Mechanism Parametric Values and Calculated Target Efficiencies	60
III. Ordinate and Cumulative Percent Values for Normal Distribution	75

EFFECTIVENESS OF A FLUIDIZED BED IN FILTRATION OF AIRBORNE PARTICULATE OF SUBMICRON SIZE

INTRODUCTION

The Problem

One of the difficulties associated with any filtration system is the removal of the collected material from the filter without shutting down the operation. Cyclones and scrubbers accomplish this by simply draining the collected material from the bottom of the system. However, most other filtration systems require periodic regeneration of the filter media; this usually necessitates taking that part of the filtration system "off the line".

If the elements of a filter can be moved readily, an arrangement becomes possible for cycling them continuously through a dust-laden stream and a cleaning system. This may make it possible to use certain materials, having desirable properties, which would not otherwise be feasible.

The fluidized bed offers an opportunity to maintain moving elements in proper position with respect to each other and the dust stream, thus producing a suitable filter media and the opportunity to regenerate the filter on a continuous basis. The purpose of this study was to investigate the factors contributing to removal efficiencies of small-diameter aerosols in a bed of fluidized glass-shot.

Independent variables were height of bed material, gas flow rate, and aerosol concentration and size.

The Selected Bed Geometry

For comparison purposes, column geometry was chosen to be essentially the same as that used by Meissner and Mickley (18). This also afforded the opportunity for measuring aerosol concentration of the entire gas stream as sampling rates could be adjusted over the range of fluidizing gas flow rates for this bed geometry.

Bed material was chosen for uniformity of sphericity, smoothness, and other characteristics. Size distribution of bed material was optimized to conform to that reported by Chakravarty et al. (3). Mean particle size was chosen to meet optimization of fluidizing characteristics indicated by Frantz (5).

In as much as other filtration systems; i. e., scrubbers, or cyclones, are reasonably effective in removing relatively large particles from the air stream, submicron particles were chosen for this study. The aerosols chosen were ammonium chloride and tobacco smoke.

LITERATURE REVIEW

Presently available references concerned with fluidized beds as filtration media or adsorbers are quite limited. However, many diverse papers present theories regarding filtration mechanisms. Some of the available references are briefly discussed in the following.

Fluidized Beds as Filtration or Adsorption Media

Meissner and Mickley (18) reported the results of laboratory experiments to investigate the possibility of using fluidized beds to remove sulfuric acid mists from an air stream. Removal efficiency of acid droplets (2-14 microns in diameter) improved with increasing bed weight per unit area and with increasing gas velocity.

Using a 1.85-inch diameter glass column, four feet high and fluidizing various bed materials, it was found that efficiencies of acid removal were independent of inlet concentration. By varying bed weight, gas velocity, and bed material, they found that the fraction of acid remaining in the effluent gas could be presented in the form,

$$\text{Ln } \frac{c_2}{c_1} = -KV_o w^n \quad (1)$$

where $K = 0.142$ and n varies from 0.157 to 0.340, depending upon the type of bed material, w is bed weight per unit area, pounds of solid per square foot, V_o is superficial gas velocity in

feet per second, and c_1 and c_2 are challenging and penetrating aerosol concentrations, respectively.

Chakravarty et al. (3) investigated the use of fluidized beds in the removal of hydrogen sulfide from coke oven gas, using an iron oxide catalyst as bed material. They report efficiencies approaching 100 percent by optimizing bed height, bed material size, and gas velocity. By replacing a portion of the used catalyst with fresh catalyst at regular intervals, continuous operation of the bed without appreciable fall in efficiency of the bed was realized.

Finding the capacity of the fluidizing bed purification unit nine to ten times higher than that of a fixed bed, Chakravarty et al. studied only the effect of the chosen independent parameters on bed life. They found increasing gas velocity reduced efficiencies at a greater rate as the bed was operated over a period of time. In other words, at a given moment in the life of the bed, lower efficiencies were found as a result of higher gas flow rates.

Filtration Mechanisms

The primary purpose of a filtration system is the disengagement or separation of the particulate phase from the carrier gas. A fundamental study of a filter requires an analysis of impaction of small particles upon the collecting media. Such an analysis must include consideration of all the forces that operate between the particles and

the collecting media. For particles of normal density in the micron and submicron range of size, the primary mechanisms by which collection may take place are:

1. Interception
2. Inertial impaction
3. Brownian diffusion
4. Electrostatic attraction
5. Settling
6. Thermal precipitation

These mechanisms are discussed in a detailed review of the literature by the American Petroleum Institute Report on Filtration (1). Some of the pertinent highlights of that and other publications are reviewed here.

Interception

Whenever the streamline along which the particle approaches a filter element passes within a distance of one-half the particle diameter from the element, interception of the particle by the filter element will occur. A limiting trajectory of this kind is shown in Figure 1. This mechanism would never occur alone except as a limiting case for particles of low density. However, it must be taken into account as a boundary condition to be met along with other filtration mechanisms.

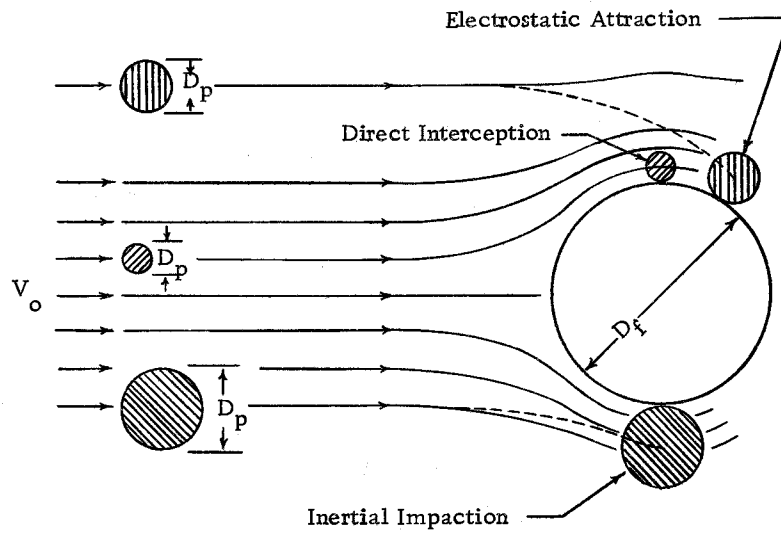


Figure 1. Streamlines and Particle Trajectories Approaching Filter Element.

Reference 1 develops a relationship for target efficiency for the direct interception of a particle by a cylinder on the basis of ideal potential flow. By defining target efficiency, η , as the ratio of cross-sectional area of fluid stream from which particles are removed to the cross-sectional area of the filter element projected in the direction of flow, it is shown that for cylindrical filter elements that

$$\eta = (1 + N_R) - \left(\frac{1}{1 + N_R} \right) \quad (2)$$

where

$$N_R = \frac{D_p}{D_f} \quad (3)$$

D_p is the aerosol diameter and D_f is the filter element diameter. Similarly, it can be shown for a spherical filter element that

$$\eta = (1 + N_R)^2 + \frac{1}{2} \left(\frac{1}{1 + N_R} \right) - \frac{3}{2} (1 + N_R) \quad (4)$$

for ideal potential flow.

Inertial Impaction

Several authors (1, 15, 19, 21, 22) have investigated target efficiencies based upon inertial impaction alone. The usual

procedure was to evaluate target efficiencies as a function of the inertial impaction parameter which arises out of the force balance equations of fluid resistance opposing the motion of the particle. The inertial impaction parameter is defined as

$$N_I = \frac{C V_o \rho_p D_p^2}{18 \mu D_f} \quad (5)$$

where C is Cunningham correction factor for Stokes' law, V_o is fluid velocity downstream, ρ_p is particle density and μ is fluid viscosity. The parameter N_I may be considered as the ratio of force necessary to stop a particle initially traveling at velocity V_o in the distance $D_f/2$, to the fluid resistance at a relative particle velocity of V_o . It is also the ratio of the distance a particle will penetrate into still gas when given an initial velocity V_o , to the diameter of the collecting medium.

Wong, Ranz, and Johnstone (22) report experimental data for inertial impaction efficiencies. Using fine wires to collect sulfuric acid droplets under such conditions that other filtration mechanisms are negligible, they obtained results for Reynolds numbers from 13 up to 330. From their work and other authors' theoretical developments, it is evident that the efficiency of collection by this mechanism is not appreciable unless the inertial impaction parameter is of the order of magnitude of at least 10^{-1} .

Brownian Diffusion

For very small particles, Brownian movement will be superimposed upon the flow motion of a particle. This relatively slow diffusional velocity may be sufficient to cause the particle to come into contact with the collector if the particle passes close enough to the filter element and remains there for a long enough time.

The authors (1, 7, 21, 22) working in this area agree that target efficiencies due to Brownian diffusion are an inverse function of the Peclet number, which arises out of the basic partial differential equation for diffusional processes.

The Peclet number defined as a function of the diffusion coefficient, D_{BM} due to Brownian diffusion is

$$N_{Pe} = \frac{V_o D_f}{D_{BM}} \quad (6)$$

The parameter N_{Pe} is the ratio of the fluid resistance to the diffusive force caused by random thermal motion. Stairmand (21) suggests the target efficiency for Brownian diffusion may be expressed as

$$\eta = \sqrt{\frac{8}{N_{Pe}}} \quad (7)$$

Others suggest similar solutions. There is fair agreement among

these solutions. There are no experimental data available, dealing with aerosols, by which these theoretical developments can be checked. However, if the value of the Peclet number is much above 100, it is felt that collection efficiencies by this mechanism would not be significant.

Electrostatic Attraction

Ranz and Wong (19) defined two parameters

$$K_E = \frac{C q_p q_f}{3\pi\mu\epsilon_o D_p V_o} \quad (8)$$

$$K_I = \frac{2}{3} \left(\frac{\epsilon_p - \epsilon_f}{\epsilon_p + 2\epsilon_f} \right) \left(\frac{CD_p^2 q_f^2}{\epsilon_o \mu V_o D_f} \right) \quad (9)$$

where ϵ_p and ϵ_f are dielectric constants of the particle and the gas and q_p and q_f are electrostatic charges for the particle and the collector. ϵ_o is permittivity of free space and μ is viscosity of the air. Equation (8) describes the interaction of a positively charged particle and collector, and equation (9) describes the interaction between a charged collector and a dielectric particle on which the collector induces a charge.

Parameters K_E and K_I may be considered ratios of the electric force at the surface of the collector to the fluid resistance

caused by a relative particle velocity of V_o with respect to the collector. It is noted that when q_p and q_f are of the same sign K_E is positive and collection efficiency decreases. Target efficiency by these mechanisms is negligible when the corresponding parameter is much less than 10^{-2} and is of the order of unity when the parameter is of the order of unity.

Kraemer and Johnstone (14) suggest that target efficiencies can be expressed for induced electrostatic attraction

$$\eta \approx \left(\frac{15\pi}{8} K_I \right)^{0.4} \quad (10)$$

and for charged particle and collector electrostatic attraction

$$\eta \approx -\pi K_E \quad (11)$$

based upon experimental data for a spherical collector.

Generalizations

Although the forces of the various mechanisms are additive, the resulting individual efficiencies are not directly additive. Each mechanism will contribute to a total efficiency, however, and no combination of favorable mechanisms will cause an efficiency lower than that expected for any one of the favorable mechanisms. In addition, the efficiency of collection for any given mechanism will be

proportional to the size of the particle and the size of the collector, and to the stream velocity in approximately the same manner that the parameter characterizing that mechanism is proportional to D_p , D_f , and V_o , by definition.

The approximate target collection efficiencies for spheres calculated by the foregoing equations are shown in Figure 2. Although the inertial mechanism is limited to collection efficiencies less than one, the electrostatic attraction mechanisms can produce collection efficiencies much greater than one. Efficiency by interception is approximately one when the aerosol size approaches that of the collector size.

Reference 1 notes that a number of workers have attempted to relate overall efficiency of a filter to theoretical target efficiencies. Unfortunately, they either apply only to a selected few of the collection mechanisms or to a limited range of parameters, or both. Probably, the only general statement that can be made at this time for the parameters discussed is

$$\eta_e = \eta(N_R, N_I, N_{Pe}, N_{Re}, K_E, K_I, \beta, h)$$

where η_e is the effective efficiency of the overall filter system, h is the height-to-diameter ratio of filter and β is the packing density.

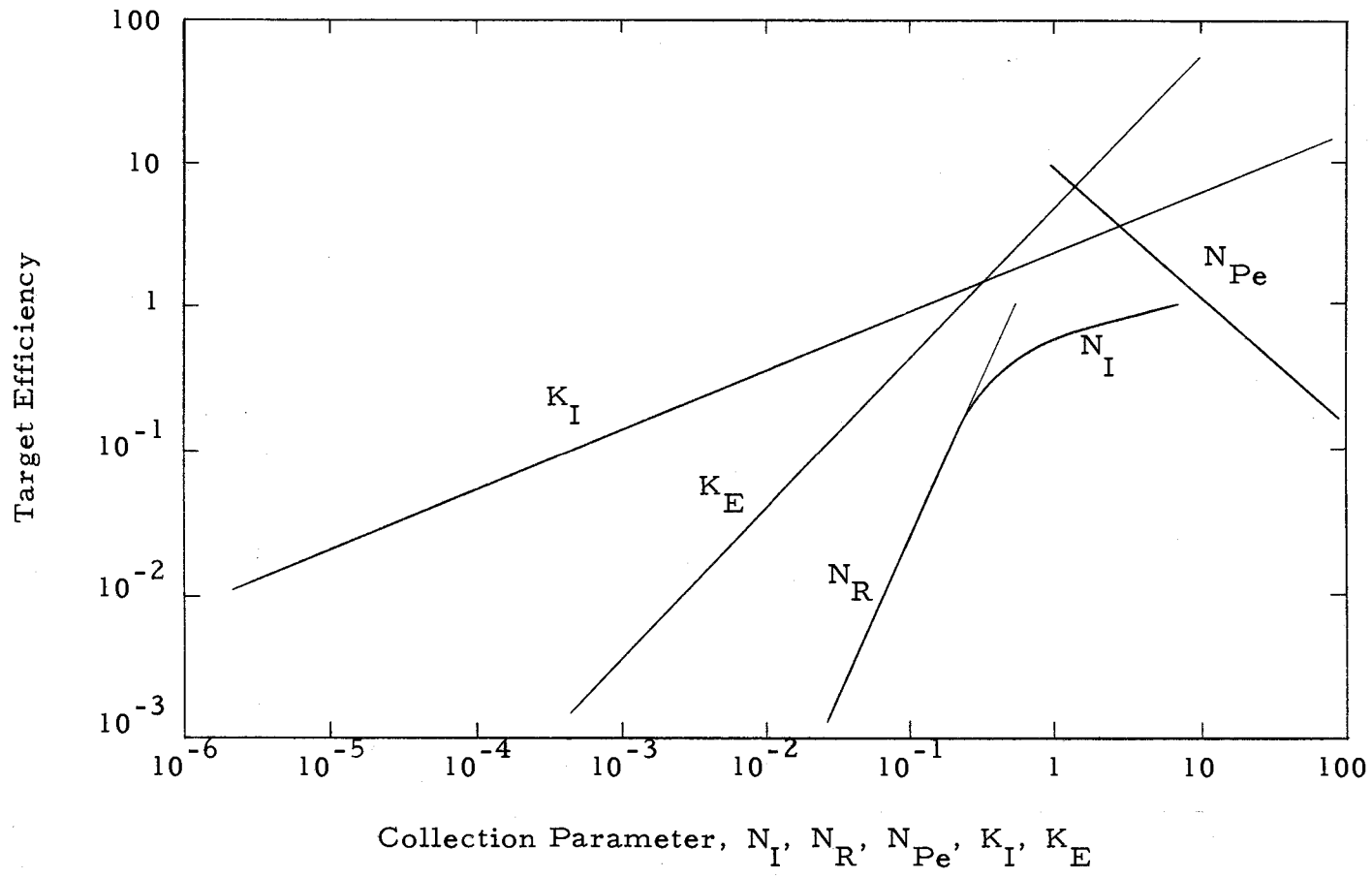


Figure 2. Approximate Solutions of Equations for Target Efficiencies.

FLUIDIZED BEDS

During the early 1940's, the first commercial fluidized process, a catalytic cracking unit, was put into use. Since that time, innumerable applications of the process have been demonstrated, many finding commercial applications. Frantz (5) lists over 25 applications of fluidized beds. Among them are catalytic cracking, process for making acetylene, evaporation of solids, vacuum retorting of oil shale, fluid cooking, fluid char adsorption process, etc. In these, the fluidized bed material functions as catalyst, reactant, heat transfer medium, drying agent, or adsorbent.

The major advantages of fluidized systems listed by Leva (17) are:

1. Continuous operation. Spent solids are easily removed from the system to be reactivated and returned to the system.
2. Flat temperature profile. Flat temperature profiles are produced due to intense particle and gas agitation.
3. High heat transfer coefficients.
4. Relatively low pressure drops through fluidized beds.
5. No special catalyst size preparation required.

Thus, a fluidized bed provides unique characteristics that may enhance many commercial applications.

Basically, fluidization describes an operation which pertains to a mode of granular solids and fluid contacting. When a column of particulate matter is subjected to an upward-directed fluid stream, the bed of solids may expand. Under certain conditions the column may exhibit properties in this state that appear to resemble some properties of liquids. The fluidized bed has no definite shape, taking the shape of its container, and is able to flow like a liquid. The bed has a definite surface with small bubbles of the fluidizing gas appearing to burst on the surface.

Fluidization of a solid particulate results when the downward-acting weight-gradient of the bed material is precisely balanced by the pressure-gradient of the gas acting upward. Figure 3a indicates the pressure-flow diagram for solids which tend to fluidize most ideally. Up to Point a, the bed is fixed. At Point a, the bed begins to expand and the pressure drop is equal to the weight-gradient of the bed.

Two common deviations from the idealized state may occur. These are channeling and slugging. Channeling is the result of non-uniform expansion of the bed in which the fluid selects certain random paths through the bed; the remainder of the bed is then left relatively uncontacted. The pressure-flow diagram of a fluidized bed undergoing channeling is shown in Figure 3b.

The other disturbance to ideal fluidized bed performance,

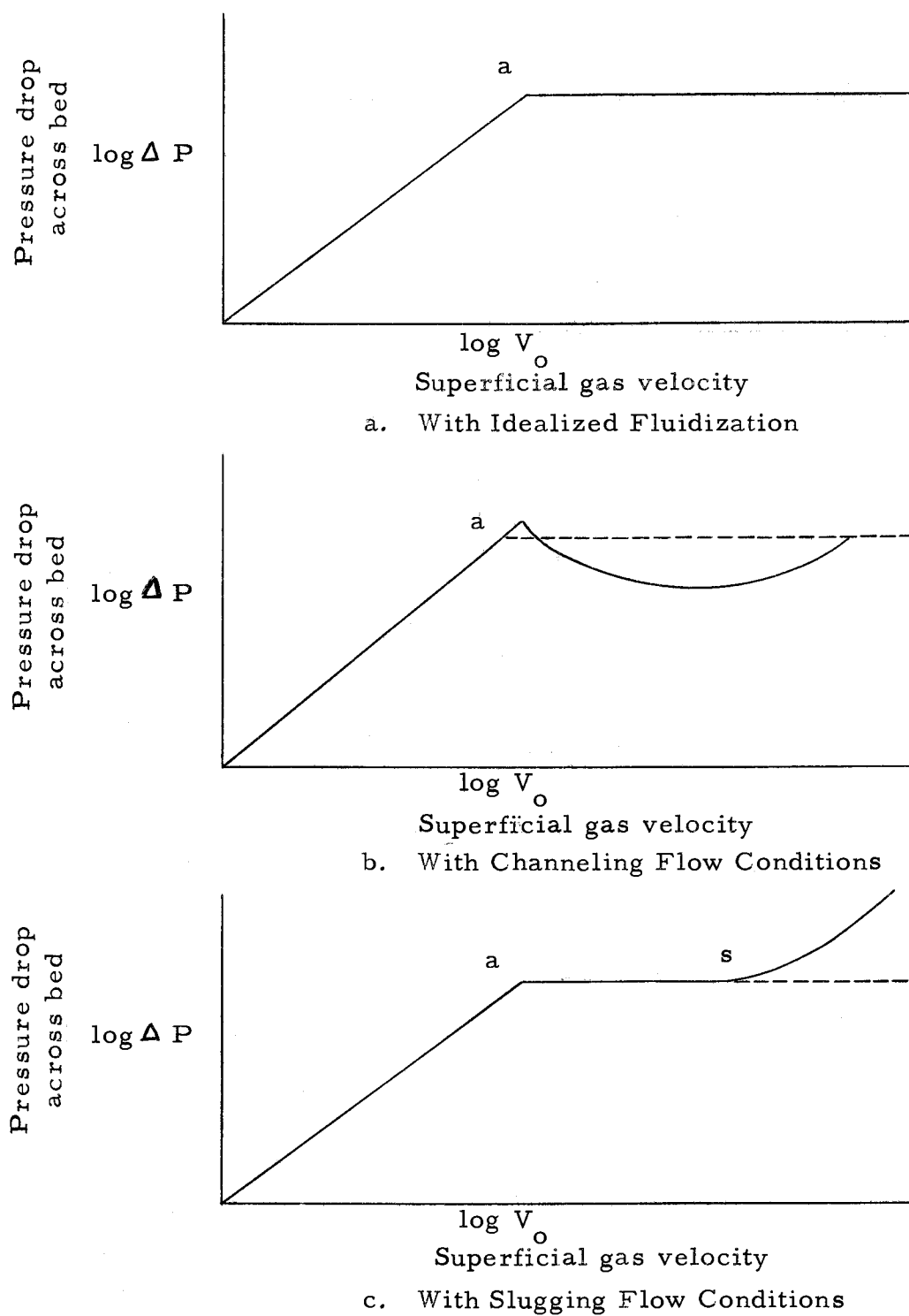


Figure 3. Pressure Drop Across Fluidized Bed vs. Superficial Gas Flow Rate.

slugging, occurs when gas bubbles of the order of magnitude of the vessel diameter coalesce. By virtue of their size, these bubbles are able to push slugs of granular solids up through the column. Slugging is usually limited to small diameter equipment and to elevated gas flow rates. Figure 3c shows the pressure-flow diagram of a slugging bed. The fluidized bed performs normally up to the Point s. At Point s, the pressure drop increases. The disadvantage of a slugging bed is its effect on space velocity and contact time.

Increasing the gas velocity through a bed of finely divided particles results in four distinct situations, depending on the geometry of the bed, characteristics of the particles, and velocity of the gas. These are: (1) fixed bed, (2) dense-phase fluidization, (3) two-phase fluidization, and (4) pneumatic transport.

As long as the pressure drop is less than the weight per unit area of the bed material, the bed remains fixed and the gas makes its way through the void spaces of the bed leaving the solid particles relatively undisturbed. This occurs at relatively low gas velocities. As the flow rate increases, a dense-phase fluidized state is reached when the pressure-gradient of the gas matches that of the bed. The bed expands and the individual particles are free to move in random motion in all directions. This condition of fluidization can be maintained indefinitely with little loss of particulate entrained in the effluent gas.

At higher velocities, two-phase fluidization occurs as a result of smaller particles being entrained in the gas stream and forming a dilute phase above the bed. The larger particles form the dense lower phase. Eventually, all of the smaller particles will be lost from the system.

Pneumatic transport occurs when the entire bed, being subjected to still higher gas velocities, is entrained with the gas. This forms a dilute phase of solid-in-gas suspension.

STIRRED SETTLING CHAMBER

A stirred settling chamber was found necessary as fluctuations in concentration occurred during sublimation of the ammonium chloride. This was considered to result from uneven heating of the flask.

The settling rate of a monodisperse aerosol in a closed chamber under turbulent conditions (stirred settling) is an exponential function of the concentration (4) which can be defined as:

$$-\frac{dc}{dt} = \frac{nv}{H} \quad (13)$$

or

$$\frac{c}{c_0} = \exp\left(-\frac{vt}{H}\right) \quad (14)$$

c = the concentration at time t

c_0 = the concentration at time zero

v = Stokes' velocity of fall for a given particle

size and density

H = the effective height of the chamber

Dimmick (4) has applied equation (14) to find particle size from light scatter decay. A straight line results when the logarithm of the concentration is plotted against time and the same slope is obtained whether c is in terms of number, geometric area, or volume (mass). A convenient procedure is to define the slope in terms of

half-life. Equation (14) can then be transferred to the linear equation

$$0.693 = \frac{v L \frac{1}{2}}{H} \quad (15)$$

Hawakawa (12) has developed a nomograph, Figure 4, which relates particle size and density to half-life for a stirred settling chamber height of 50 centimeters.

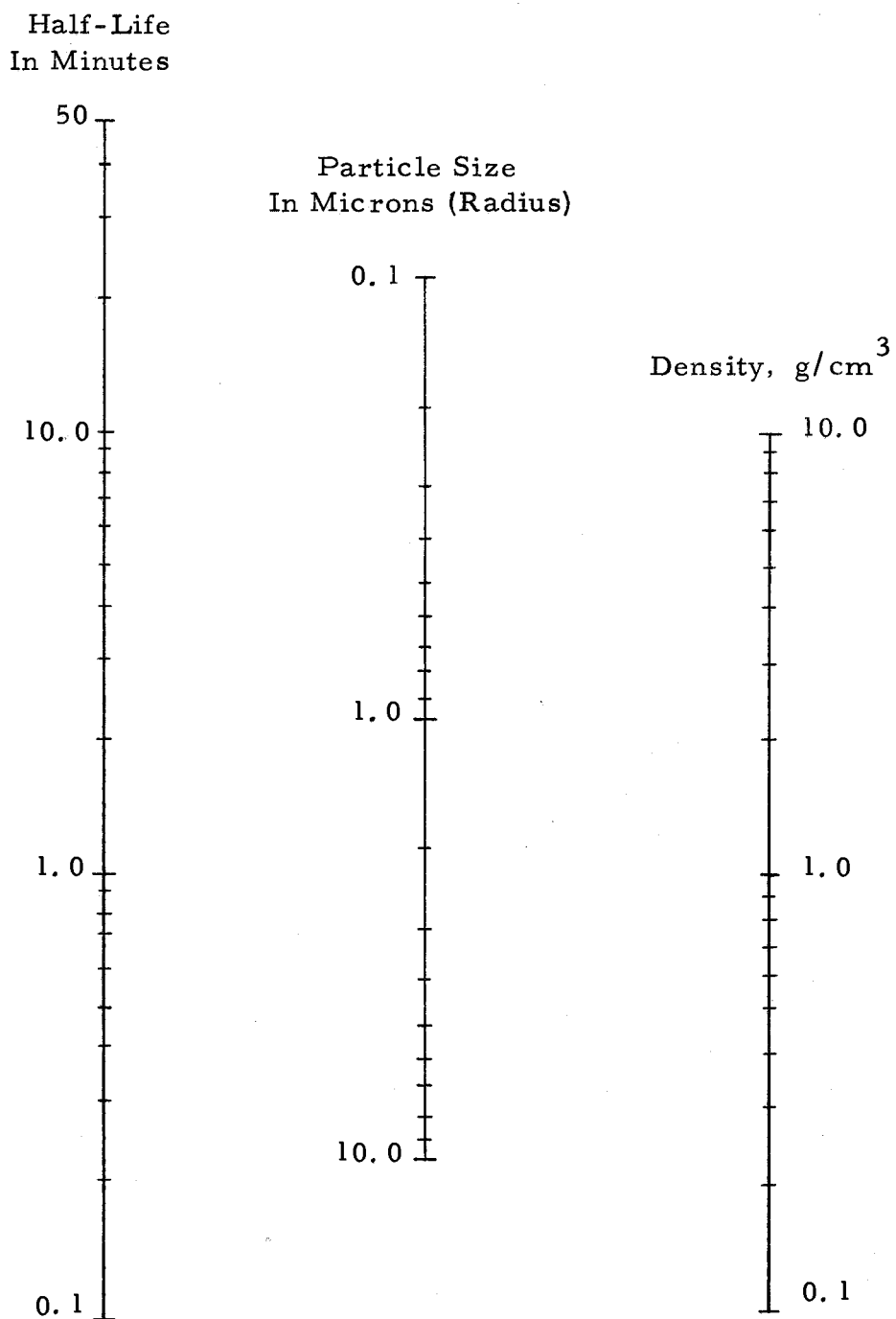


Figure 4. Nomograph for use in Calculating Stokesian Radius from Half-Life Data (Chamber Height 50 cm.).

EXPERIMENTAL PROGRAM

Scope

The effectiveness of a fluidized bed in removing airborne particulate from an air stream was investigated at superficial gas velocities of 8.75 to 25.0 feet per minute. Lower velocities were insufficient to fluidize the bed material, while higher velocities resulted in excessive bed carry-over. Bed height-to-diameter ratios were varied from two to six. Concentrations of aerosol ranged from 0.03 to 8.3 milligrams per cubic meter. Ambient temperature conditions prevailed, normally 20° C to 30° C.

Experimental Apparatus

Overall Description

The apparatus used is shown in Figures 5 and 6. Room air, after passing through a filter, entered the aerosol generating flask. There, sublimated ammonium chloride particles were picked up in the air stream and carried to the stirred-settling chamber. The chamber entrance valve was shut off and the vacuum pump pulled air from the stirred settling chamber through the fluidized column and photometer. The four-way reversing valve allowed the column to be shunted out of the system and the air stream to go directly to the photometer,

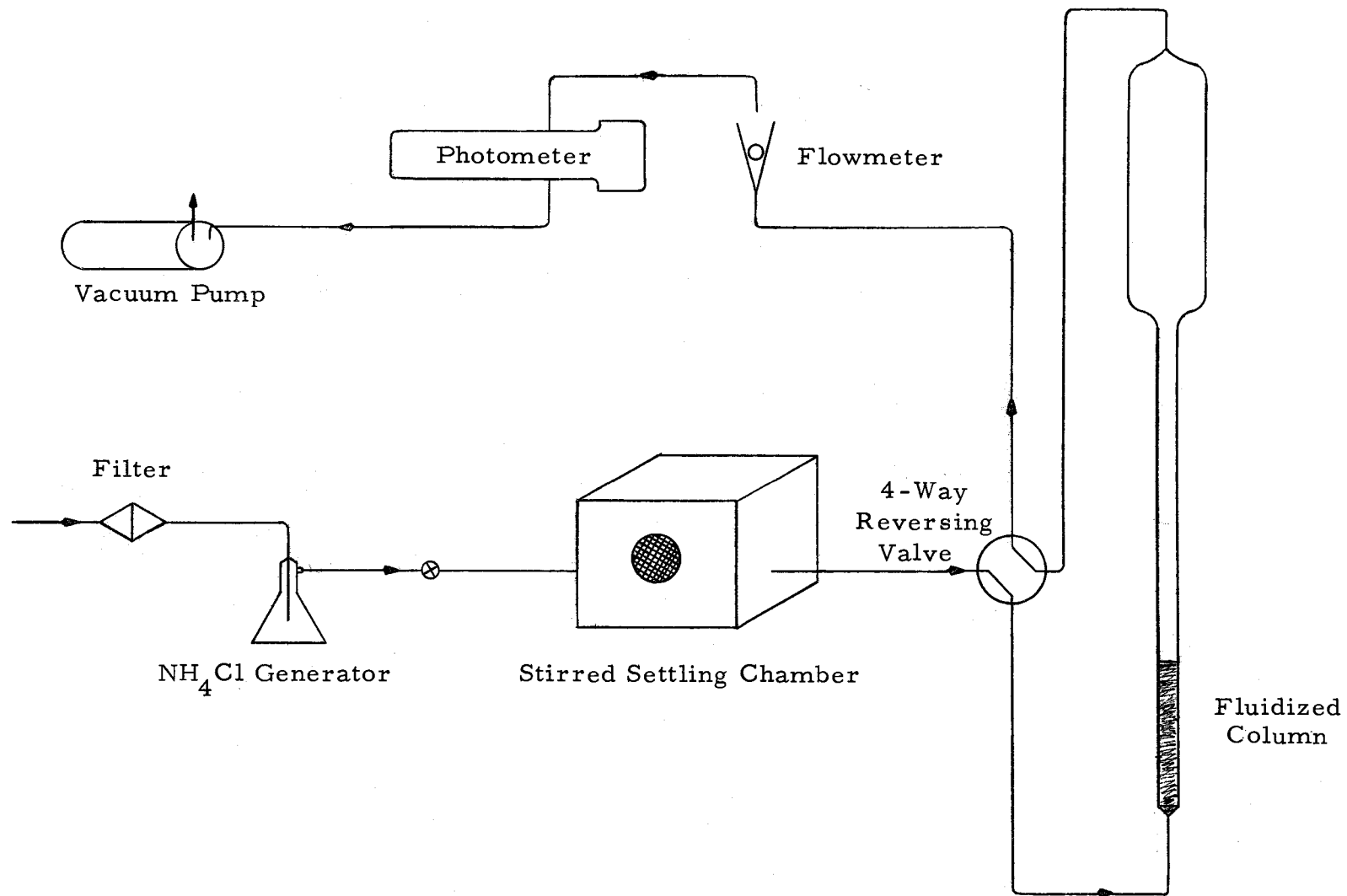


Figure 5. Schematic Flow Diagram.

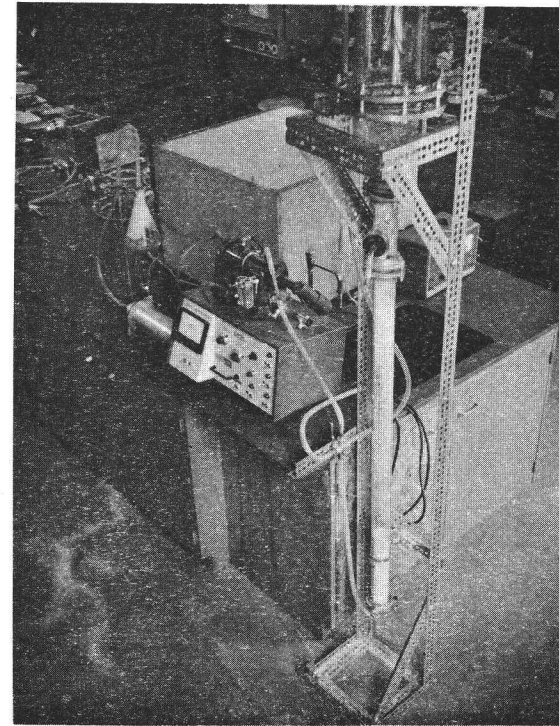
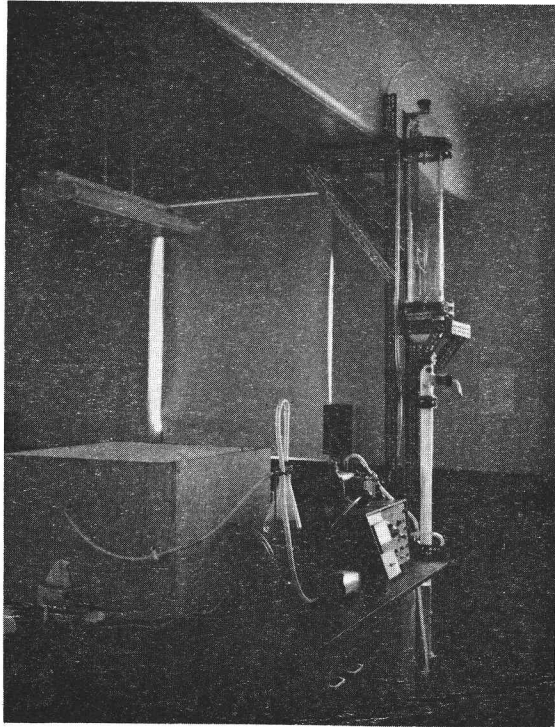


Figure 6a. Apparatus for Determining Filtration Efficiencies of a Fluidized Bed, Generalized Views.

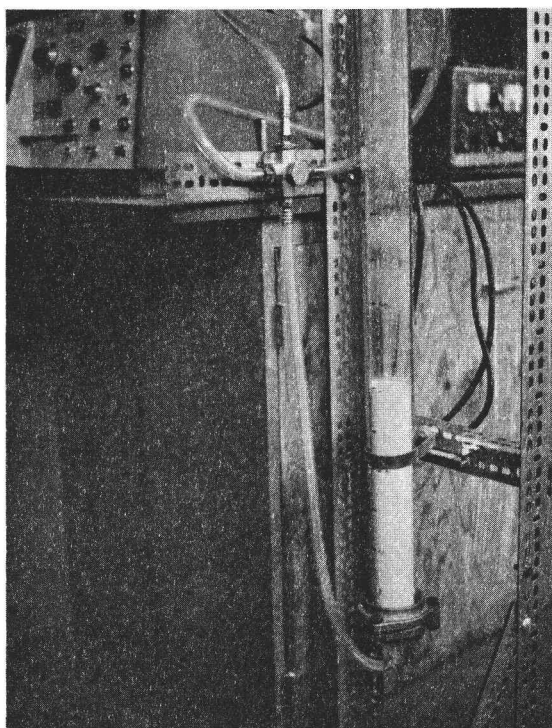


Figure 6b. Apparatus for Determining Filtration Efficiencies of a Fluidized Bed, Fluidizing Column and Four-way Reversing Valve.

bypassing the column. Thus, mass concentrations of the aerosol penetrating the system could be compared with the mass concentration of the challenging aerosol by switching the reversing valve position.

Aerosol Generator

An aerosol was generated by sublimating ammonium chloride (Sal Ammoniac) powder in a heated (340° C) flask. As the ammonium chloride gas cooled and recondensed, the subsequent particulate was carried to the stirred settling chamber by filtered air. The mean size of the ammonium chloride particulate generated was determined by light field microscopy to be 0.56 microns, with a geometric deviation of 2.83. Specific gravity of the particulate was 1.527. The particulate was spherical in shape and translucent in color.

Stirred Settling Chamber Assembly

A stirred settling chamber was constructed of one-half-inch plywood, 50 centimeters high by $73\frac{3}{4}$ centimeters square, providing a volume of 292 liters. A three-inch d-c fan was located ten centimeters from the bottom center. Entrance and exit hose fittings were located about half-way up the side of the chamber on adjacent sides. Three layers of one-half-inch thick fiber-glass filter media filtered air entering the chamber through a three-inch hole in the side of the chamber. This filter media provided essentially 100 percent

efficiency in removing any air borne particulate from the room air.

Fluidized Bed Assembly

The fluidized bed utilized in this study consisted of a four-foot long pyrex glass column with an inside diameter of two inches. Above this column was placed a 30-inch section, six inches in diameter, to act as a settling chamber for any particulate that may have become entrained in the gas stream. The fluidizing gas entered at the bottom of the two-inch column through a simple 60° cone, passing through the bed, entering the six-inch disengaging section and passing out through a fitting at the top. No gas diffuser plate was used to support the bed material as this would become plugged with the aerosol concentrations used in this study. This arrangement made the bed similar to a spouting bed as described by Leva (17).

The bed material was glass-shot with a mean size of 25.5 microns and geometric deviation of 1.70 (Figure 7). Over 85 percent to the glass-shot was spherical in shape. Density of the shot was 2.99 grams per cubic centimeter.

Aerosol Photometer

A Sinclair-Phoenix Aerosol, Smoke, and Dust Photometer, Model JM2000, was used to measure aerosol concentrations of challenging and penetrating aerosols. This photometer indicated aerosol

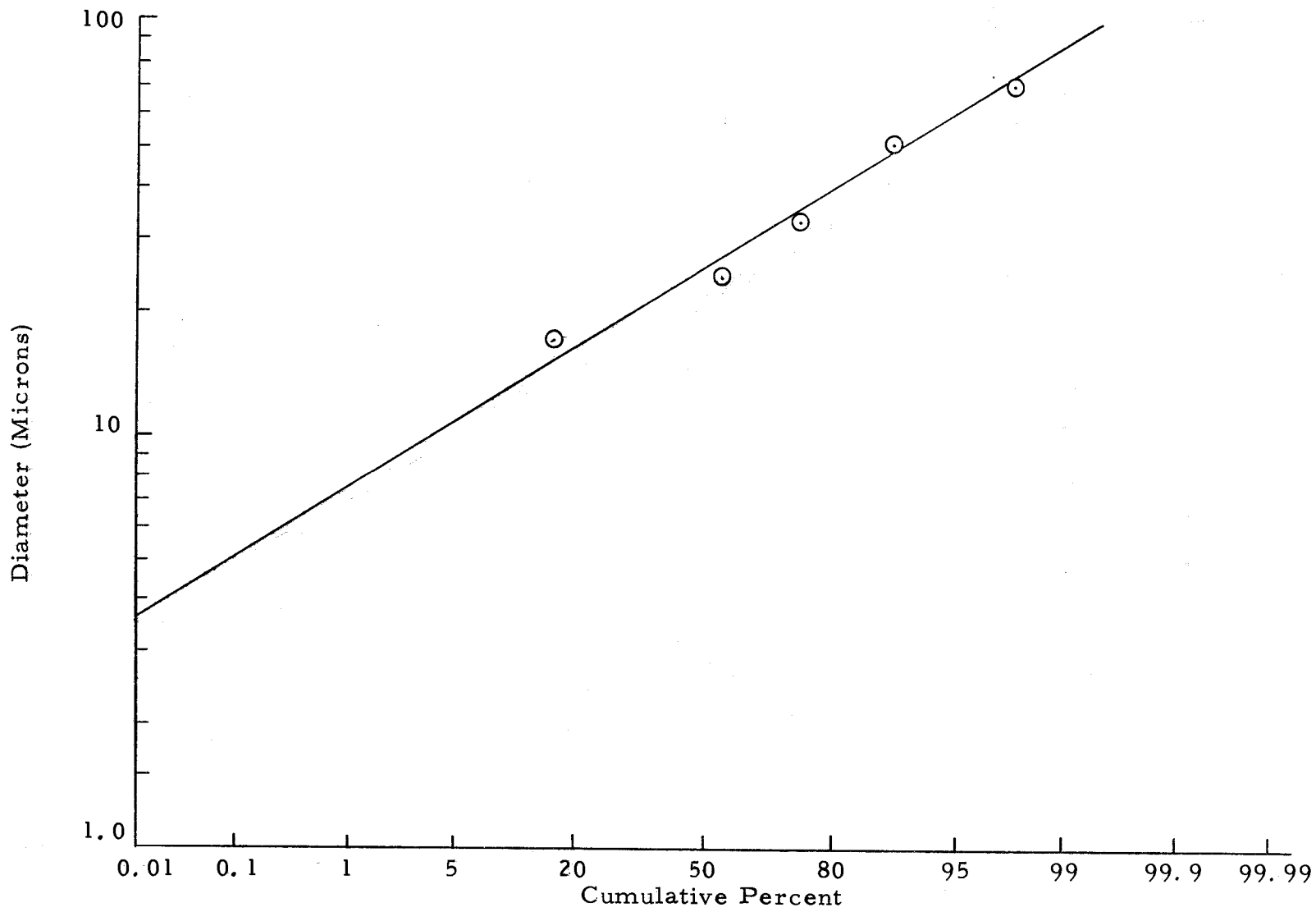


Figure 7. Fluidized Bed Material Size Distribution, Logarithmic Probability Graph.

concentration at any instant by the measurement of small-angle, forward-scattering light. Flow meters, which had been calibrated by a "precision" wet test gas meter, on the photometer regulated the gas flow rate through the fluidized bed. A Gast Manufacturing Corporation vacuum pump, model 0321-V30, provided driving force for gas movement through the system.

Experimental Procedures

Upon charging the stirred settling chamber with an aerosol, a suitable period (5-15 minutes) was allowed to lapse for the larger particles of the aerosol to settle out. After this period, the fluidized bed was challenged by the aerosol from the chamber. A transition period followed until the fluidized bed and column reached a steady state. Figure 8 shows a typical transition period where the percent penetration of the column by the aerosol increased from background noise level to a steady state.

The entire effluent gas stream from the fluidized bed was carried through Tygon tubing to the photometer which measured the concentration of the aerosol remaining in the gas stream after passing through the fluidized bed. The concentration of the challenging aerosol was measured by diverting the flow from entering the bed to the photometer by means of a four-way reversing valve. The photometer was calibrated prior to each series of runs. Figure 9 is a typical

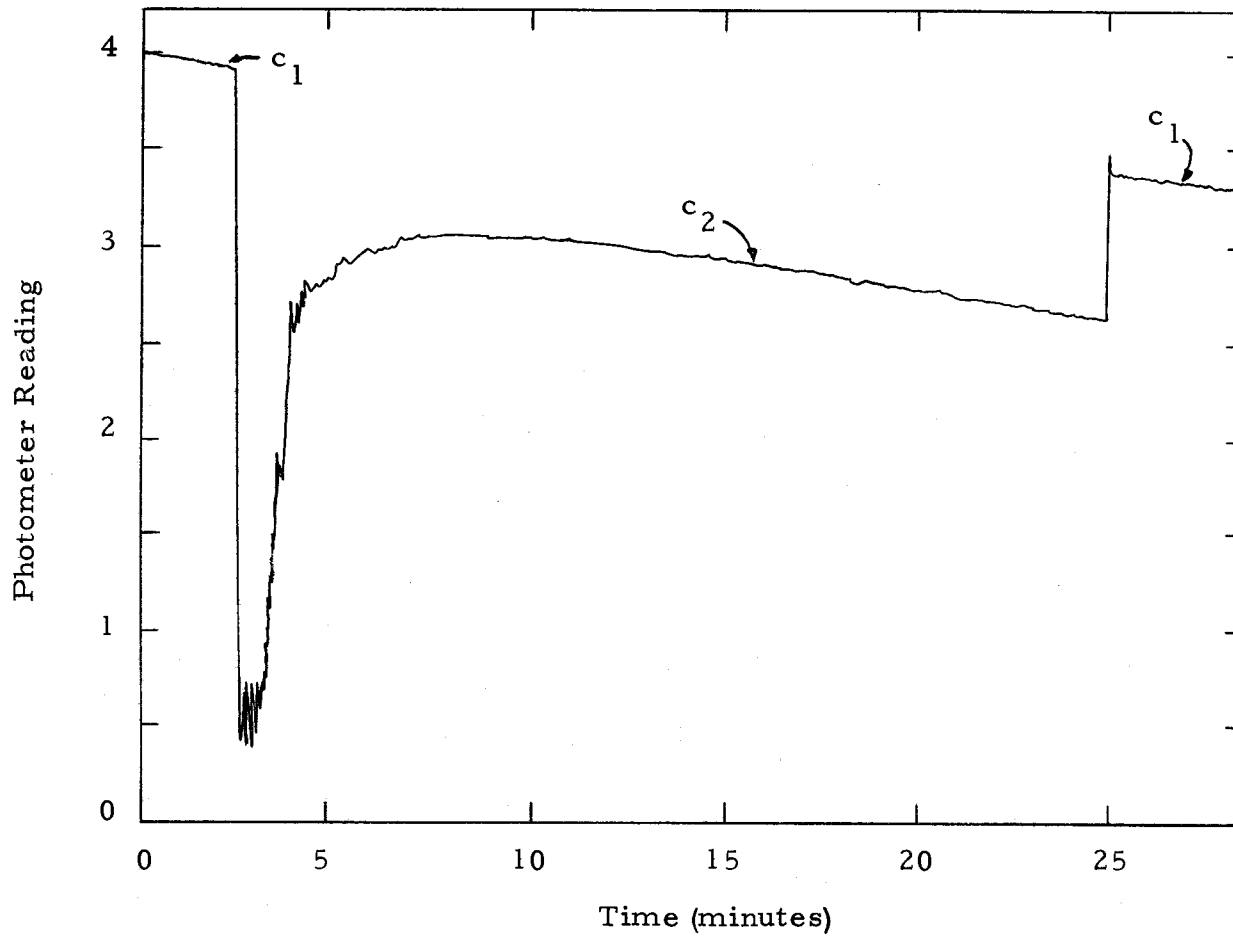


Figure 8. Recording Trace of Photometer Read-Out vs. Time.
 c_1 Indicates Reading While Sampling Challenging Aerosol;
 c_1^1 Indicates Reading While Sampling Penetrating Aerosol.

calibration curve for the photometer. As concentration of the aerosol in the stirred settling chamber was a function of time, a series of measurements of challenging and penetrating aerosol concentrations were made over a period of time for each variation of bed height or flow rate. This provided the data required for determining the mean aerosol size and the effectiveness of the fluidized bed as a function of challenging aerosol concentration.

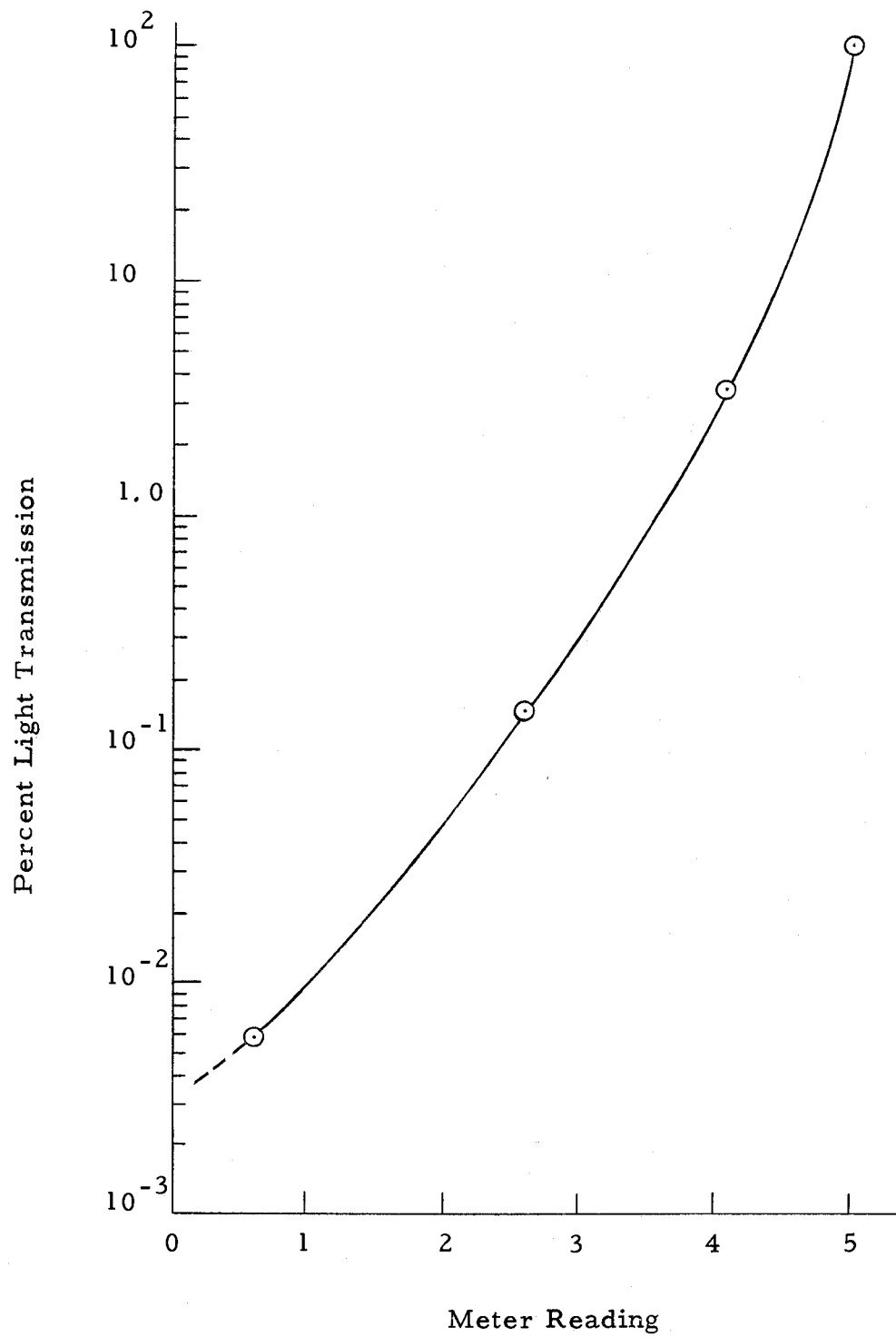


Figure 9. Aerosol Photometer Calibration Graph.

RESULTS

The following discussion is a presentation of the results of the studies relating to submicron filtration efficiencies of a fluidized bed. The studies include fluidized bed performance as a function of bed height, gas flow rates, aerosol concentration and size distribution.

Table I indicates the results collected during the study. The time variation of concentration of challenging and penetrating aerosols for runs utilizing ammonium chloride as an aerosol are shown in Figures 10-21, inclusive. Standard deviation of data was 0.025.

Light field microscopy was used to determine the challenging aerosol particle size distribution (Figure 22). The mean size with respect to count was 0.52 microns with a geometric deviation of 2.32. Mean size with respect to mass was 4.3 microns as determined by the following relationship suggested by Hatch (11).

$$\ln N_m = \ln N_n + 3 \ln^2 \sigma_g \quad (16)$$

Tobacco smoke was determined by light field microscopy to have a mean size of 0.35 microns. However, it is felt that this determination was too low since water and certain soluble organics which surrounded the tobacco particle did not show up in the method of microscopy. Tobacco particle diameter is estimated to be the same as ammonium chloride particles, inasmuch as filtration efficiencies

were almost exactly the same under the same conditions of operating variables.

Pressure drop across the fluidized bed was measured with a water manometer. Figure 23 indicates pressure drops for several different bed heights as a function of gas flow rates. The characteristic shape of these curves indicates slugging was present in the fluidized bed, particularly at low bed heights and high gas flow rates. Dense phase fluidization occurred in all tests.

As the aerosol in the stirred settling chamber was withdrawn at a constant rate and the remaining aerosol was being diluted by filtered air, equation (14) is modified by this dilution rate to

$$\frac{n}{n_0} = \exp \left(-\frac{vt}{H} - \frac{Qt}{A} \right) \quad (17)$$

where Q is the flow rate of the aerosol being withdrawn from the chamber, and A is the volume of the chamber. Equation (15) then becomes

$$0.693 = \left(\frac{v}{H} + \frac{Q}{A} \right) L_{\frac{1}{2}} \quad (18)$$

By solving equation (18) for various flow rates and using Figure 4, the mean aerosol diameter was found to be of the order of one micron. However, it should be noted that the stirred settling chamber did not produce a true monodisperse particulate. This may be due

to the fact that percent of the particulate was within 0.6 microns of the mean size, and the method of the stirred settling chamber was unable to distinguish this small variation in size.

Filtration efficiencies of the fluidized bed in removing either ammonium chloride or tobacco particles of submicron size ranged from approximately 50 to 90 percent on a count basis. Lowest efficiencies were encountered at highest gas flow rates and lowest bed heights. Highest efficiencies resulted from low gas flow rates and high bed heights. No effective change in filtration efficiencies of the fluidized bed were found as a result of bed age or changes in challenging aerosol concentration. Figure 24 shows efficiency data for several combinations of bed height and gas flow rates as a function of inlet concentration of the aerosol. It was found that the following equation could fit the data for all runs within experimental accuracies.

$$\eta_e = 0.565 \frac{h^{0.4}}{V_o^{0.1}} \quad (19)$$

where h is the bed height-to-diameter ratio and V_o is the superficial gas velocity. Figure 25 indicates this relationship. Over 90 percent of measured efficiency values are within 5 percent of values predicted by equation (19). Figure 26 presents efficiency data (means) as a function of $h^{0.4}/V_o^{0.1}$.

Table I. Results of Fluidized Bed Filtration Efficiency Measurements

No.	Bed Height-to-Diameter Ratio, h	Superficial Gas Velocity V_0 (Ft/Min)	Percent Light Transmission Penetrating Aerosol	Percent Light Transmission Challenging Aerosol	Effective Filter Efficiency, η_e
1	2	8.75	2.00	5.10	0.608
2			1.15	3.40	0.661
3			0.87	2.38	0.634
4			0.60	1.50	0.600
5			0.59	1.48	0.602
6			0.46	1.18	0.610
7			0.39	1.00	0.610
8			0.31	0.83	0.626
9			0.265	0.69	0.616
10			0.19	0.47	0.596
11			0.13	0.335	0.612
12			0.11	0.28	0.607
13			1.40	3.75	0.626*
14			1.10	3.00	0.632*
15			0.84	2.30	0.634*
16		10.96	0.54	1.28	0.578
17			0.37	0.79	0.532
18			0.275	0.65	0.577
19			0.23	0.53	0.566
20			0.20	0.425	0.529
21			0.17	0.365	0.534
22			0.13	0.29	0.552
23			0.11	0.25	0.560
24			0.081	0.19	0.573
25			0.053	0.125	0.576
26			0.036	0.086	0.581
27			0.0305	0.074	0.588
28			1.51	4.00	0.622*
29			0.54	1.45	0.628*
30			0.50	1.30	0.614*
31		14.65	1.00	2.30	0.564
32			0.69	1.50	0.539
33			0.56	1.25	0.553
34			0.48	1.15	0.582

Table I. cont.

No.	Bed Height-to-Diameter Ratio, h	Superficial Gas Velocity V_0 (Ft/Min)	Percent Light Transmission Penetrating Aerosol	Percent Light Transmission Challenging Aerosol	Effective Filter Efficiency, η_e	
35	2	14.65	0.36	0.87	0.586	
36			0.23	0.55	0.582	
37			0.14	0.30	0.532	
38			0.096	0.235	0.592	
39			0.088	0.20	0.560	
40			0.068	0.15	0.548	
41			0.0365	0.85	0.571	
42			0.0240	0.55	0.563	
43			1.65	4.00	0.590*	
44			0.37	0.90	0.589*	
45			0.245	0.60	0.591*	
46			25.00	1.05	2.15	0.511
47				0.75	1.55	0.516
48				0.50	1.10	0.546
49		0.39		0.85	0.520	
50		0.325		0.67	0.514	
51		0.30		0.60	0.500	
52		0.225		0.50	0.550	
53		0.19		0.38	0.500	
54		0.16		0.31	0.484	
55		0.12		0.24	0.500	
56		0.103		0.20	0.485	
57		0.077		0.155	0.504	
58		0.064		0.12	0.467	
59		0.051		0.10	0.490	
60		1.51	3.75	0.507*		
61		0.118	0.245	0.518*		
62		0.078	0.18	0.567*		
63		3	8.75	1.05	4.30	0.756
64			8.75	0.95	3.90	0.756
65			8.75	0.80	3.10	0.742
66			10.96	0.65	2.45	0.734
67	10.96		0.55	2.00	0.725	
68	10.96		0.38	1.51	0.748	
69	14.65		0.30	1.00	0.700	
70	14.65		0.245	0.76	0.678	
71	14.65		0.20	0.69	0.710	
72	25.00		0.17	0.53	0.678	
73	25.00		0.15	0.94	0.659	
74	4		25.00	0.125	0.37	0.662
75			8.75	0.058	0.38	0.847

Table I. cont.

No.	Bed Height-to-Diameter Ratio, h	Superficial Gas Velocity V_0 (Ft/Min)	Percent Light Transmission Penetrating Aerosol	Percent Light Transmission Challenging Aerosol	Effective Filter Efficiency, η_e
76	4	8.75	0.052	0.33	0.842
77		8.75	0.041	0.26	0.842
78		8.75	0.036	0.235	0.847
79		8.75	0.380	1.90	0.805*
80		8.75	0.315	1.55	0.797*
81		8.75	0.270	1.38	0.804*
82		8.75	0.215	1.05	0.796*
83		10.96	0.415	1.85	0.775
84			0.270	1.09	0.734
85			0.200	0.77	0.740
86			0.128	0.52	0.754
87			0.900	0.38	0.763
88			0.050	0.21	0.762
89			0.70	3.70	0.712*
90			0.57	2.80	0.797*
91			0.52	2.50	0.792*
92			0.45	0.65	0.777*
93			0.125	0.59	0.788*
94		14.65	0.35	1.37	0.744
95			0.32	1.22	0.737
96			0.26	0.99	0.738
97			0.21	0.84	0.750
98			0.17	0.68	0.749
99			0.109	0.415	0.737
100			0.090	0.34	0.736
101			0.31	1.25	0.757*
102			0.21	1.00	0.790*
103			0.171	0.70	0.755*
104			0.140	0.63	0.778*
105			0.111	0.48	0.768*
106		25.00	0.80	2.95	0.729
107			0.60	2.45	0.755
108			0.43	1.70	0.747
109			0.345	1.34	0.743
110			0.265	1.02	0.740
111			0.212	0.80	0.735
112			0.150	0.57	0.736
113			0.115	0.43	0.732
114			0.072	0.265	0.729
115			0.046	0.165	0.721
116			0.032	0.130	0.715

Table I. cont.

No.	Bed Hight-to-Diameter Ratio, h	Superficial Gas Velocity V_0 (Ft/Min)	Percent Light Transmission Penetrating Aerosol	Percent Light Transmission Challenging Aerosol	Effective Filter Efficiency, η_e
117	4	25.00	1.05	4.00	0.737*
118			0.82	3.10	0.735*
119			0.70	2.60	0.730*
120			0.55	2.05	0.732*
121	6	8.75	0.25	2.0	0.895
122			0.135	1.2	0.887
123			0.081	0.80	0.899
124			0.054	0.48	0.888
125			0.036	0.36	0.900
126			0.440	4.40	0.900*
127			0.365	3.75	0.925*
128			0.360	3.60	0.900*
129		10.96	0.43	3.7	0.884
130			0.38	2.8	0.864
131			0.13	1.25	0.896
132			0.096	0.86	0.888
133			0.084	0.72	0.883
134			0.046	0.47	0.902
135			0.34	2.6	0.869*
136			0.31	2.5	0.876*
137			0.235	2.1	0.888*
138			0.215	2.0	0.892*
139		14.65	0.18	1.13	0.842
140			0.116	0.77	0.849
141			0.086	0.60	0.857
142			0.053	0.34	0.844
143			0.039	0.25	0.844
144			0.0238	0.158	0.850
145			0.20	1.3	0.846*
146			0.175	1.15	0.848*
147			0.150	0.98	0.847*
148		25.00	0.41	1.78	0.770
149			0.235	1.1	0.786
150			0.178	0.87	0.795
151			0.081	0.39	0.792
152			0.058	0.295	0.800
153			0.160	0.86	0.814*
154			0.126	0.70	0.840*
155			0.117	0.67	0.825*

*Tobacco smoke

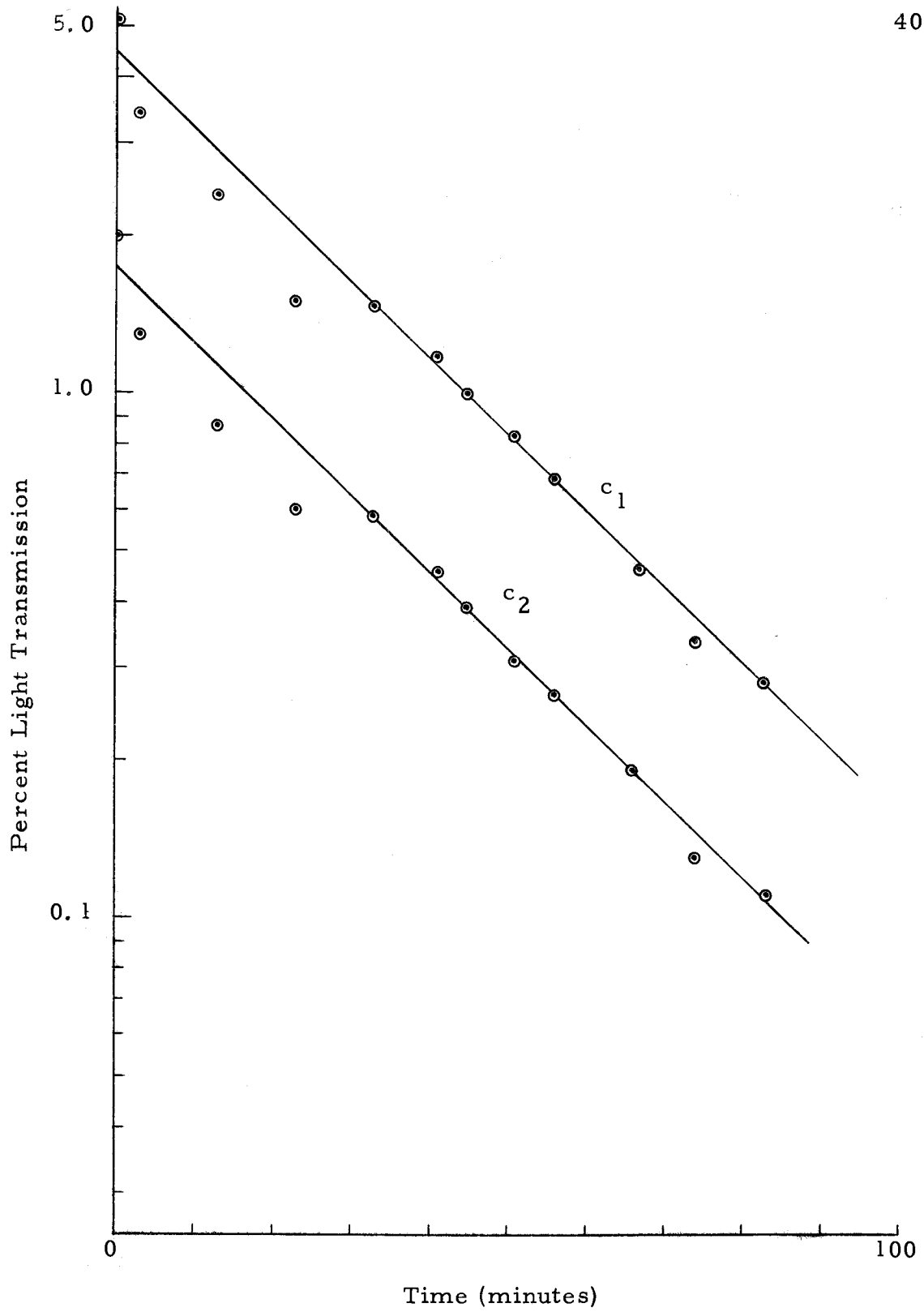


Figure 10. Percent Light Scatter vs. Time for Challenging Aerosol, c_1 and Penetrating Aerosol, c_2 , $h = 2$, $V_0 = 8.75$ ft/min.

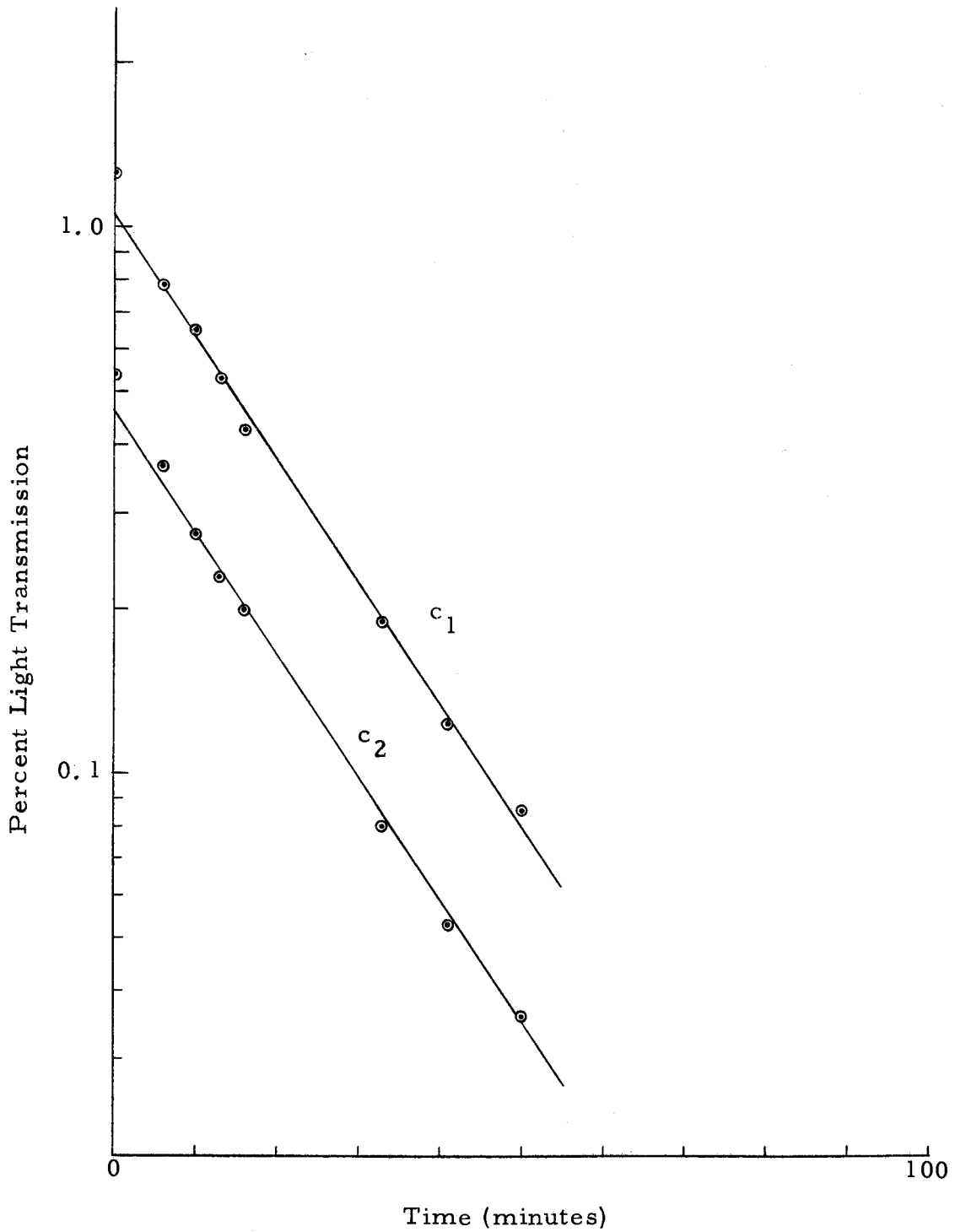


Figure 11. Percent Light Scatter vs. Time for Challenging Aerosol, c_1 and Penetrating Aerosol, c_2 . $h = 2$, $V_o = 10.96$ ft/min.

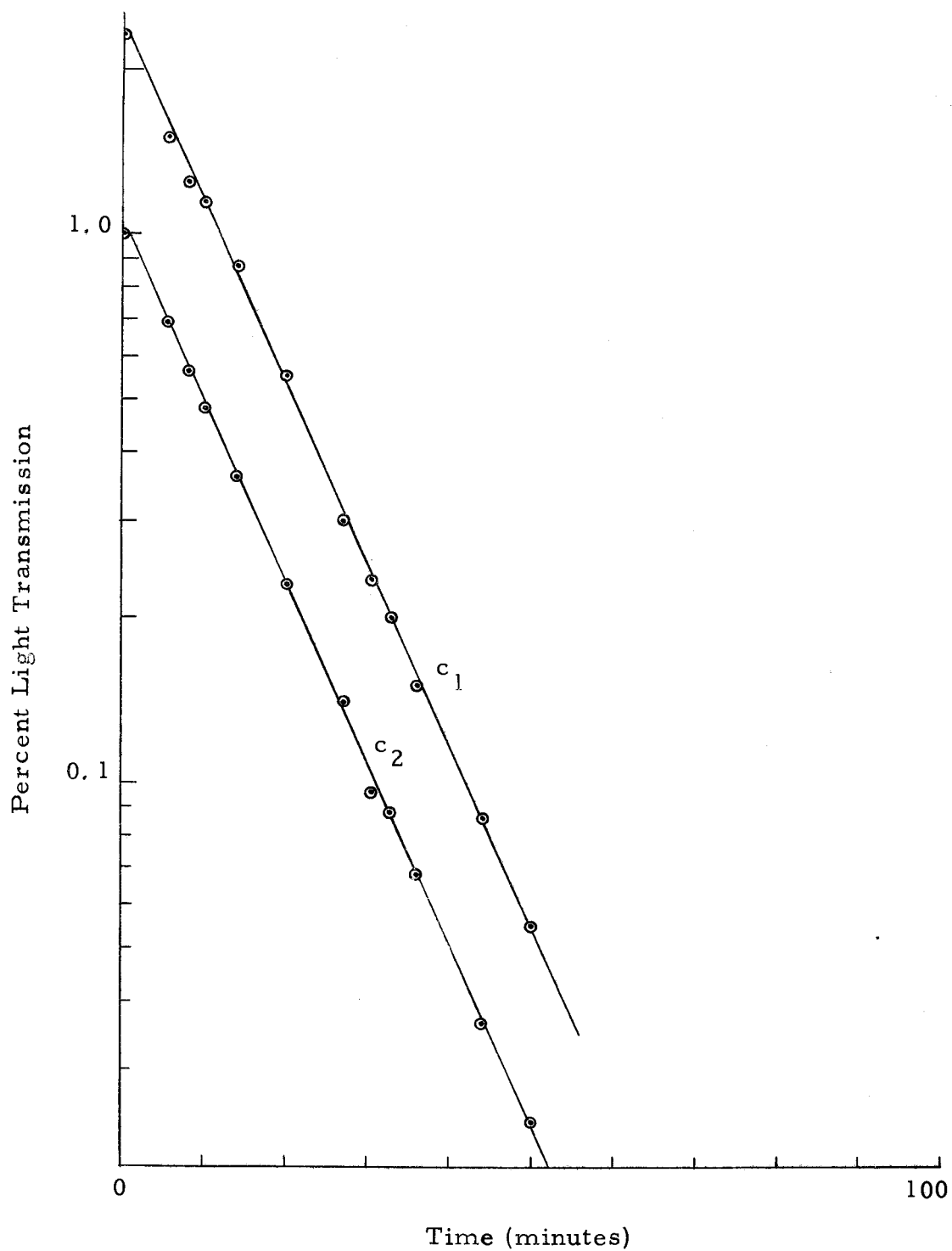


Figure 12. Percent Light Scatter vs. Time for Challenging Aerosol, c_1 and Penetrating Aerosol, c_2 . $h = 2$, $V_o = 14.65$ ft/min.

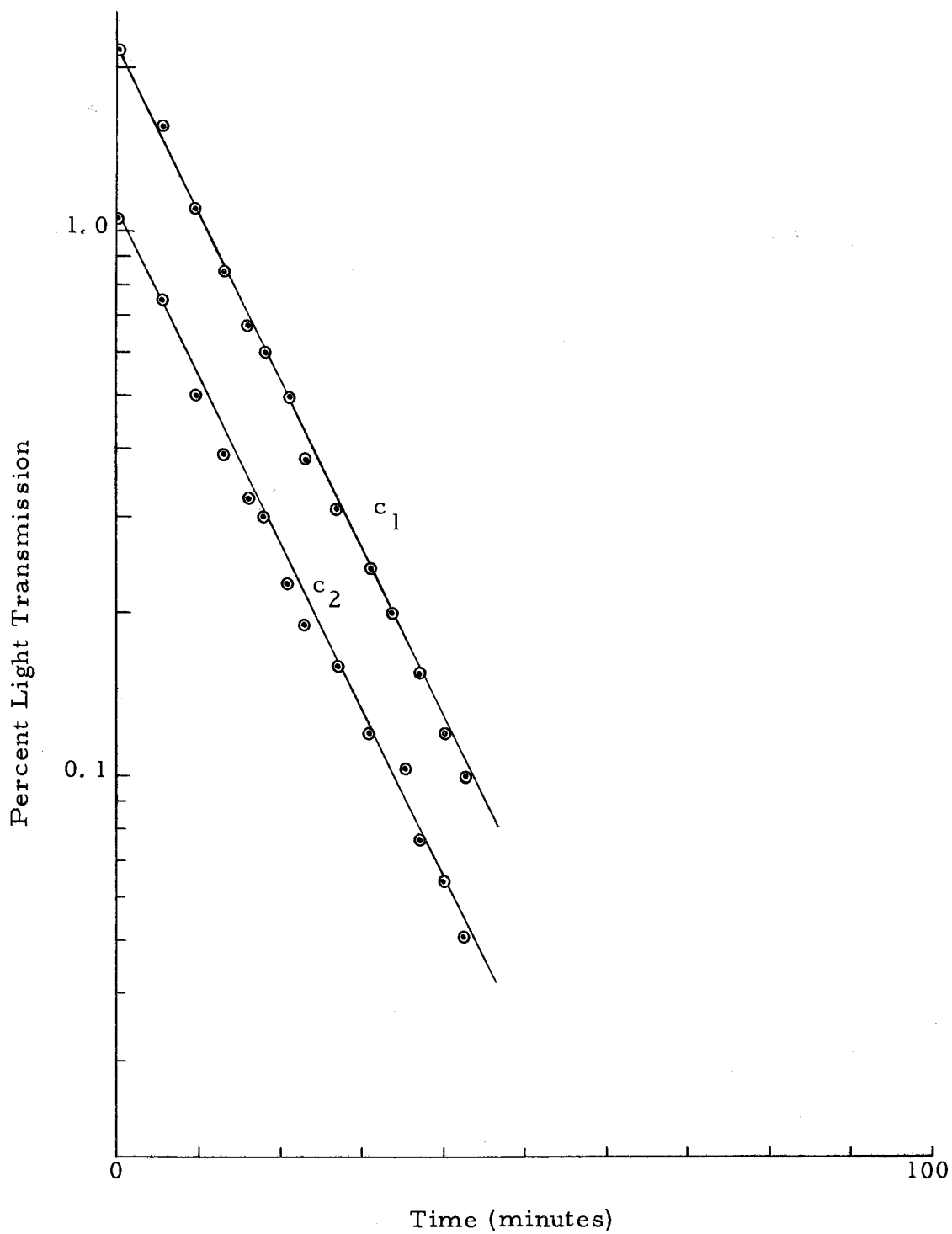


Figure 13. Percent Light Scatter vs. Time for Challenging Aerosol, c_1 and Penetrating Aerosol, c_2 . $h = 2$, $V_o = 25.00$ ft/min.

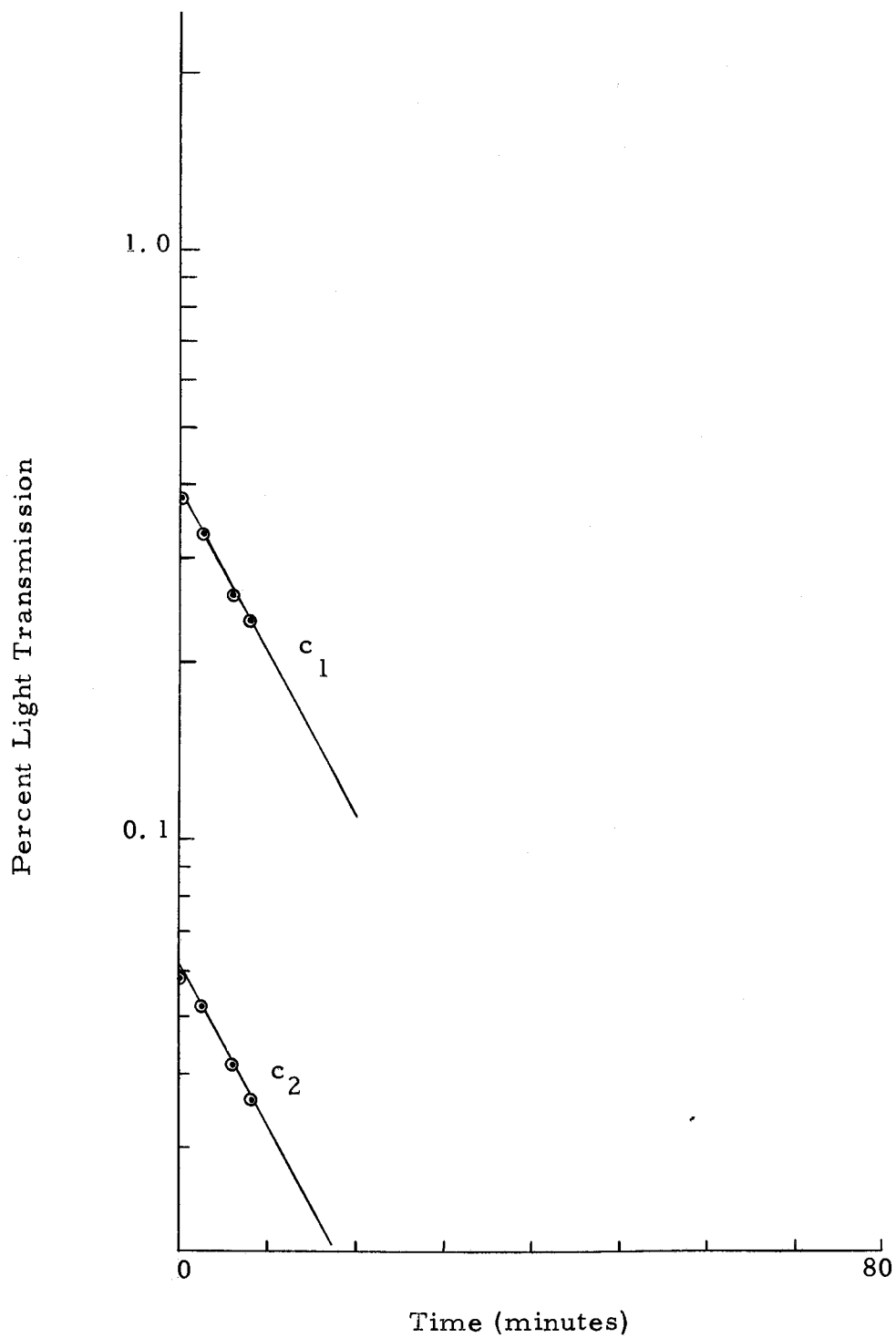


Figure 14. Percent Light Scatter vs. Time for Challenging Aerosol, c_1 and Penetrating Aerosol, c_2 . $h = 4$, $V_o = 8.75$ ft/min.

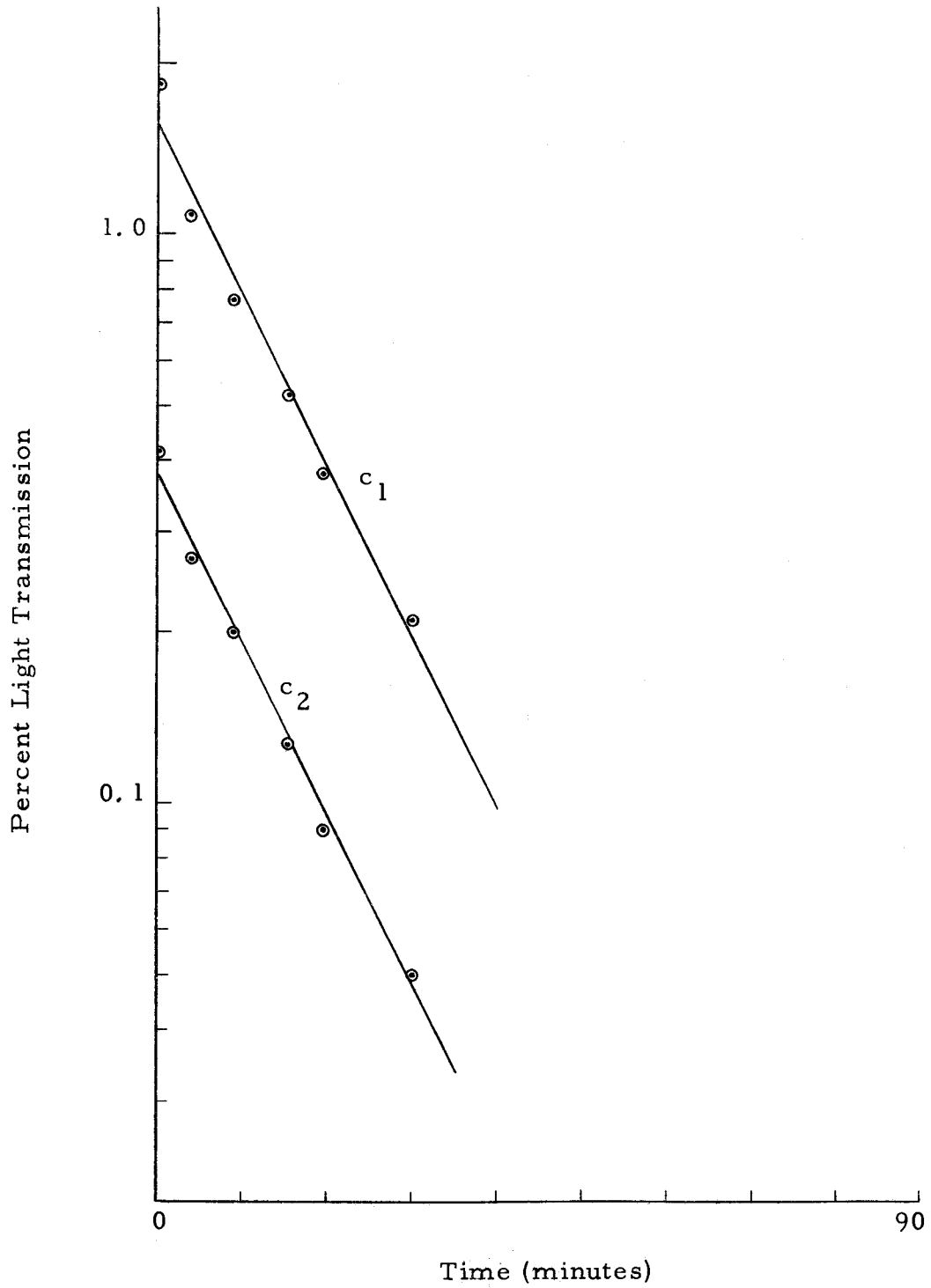


Figure 15. Percent Light Scatter vs. Time for Challenging Aerosol, c_1 and Penetrating Aerosol, c_2 . $h = 4$, $V_o = 10.96$ ft/min.

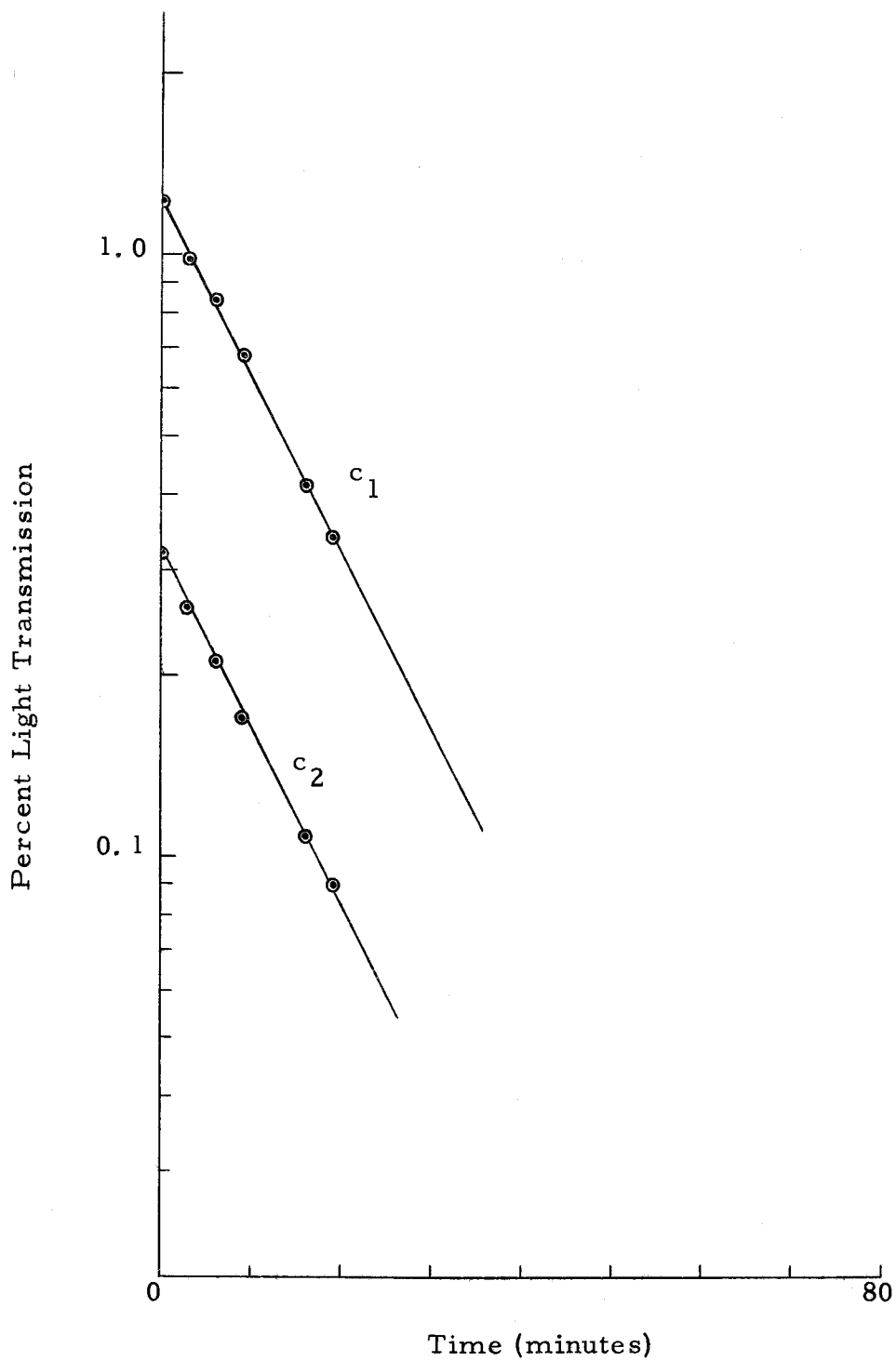


Figure 16. Percent Light Scatter vs. Time for Challenging Aerosol, c_1 and Penetrating Aerosol, c_2 . $h = 4$, $V_o = 14.65$ ft/min.

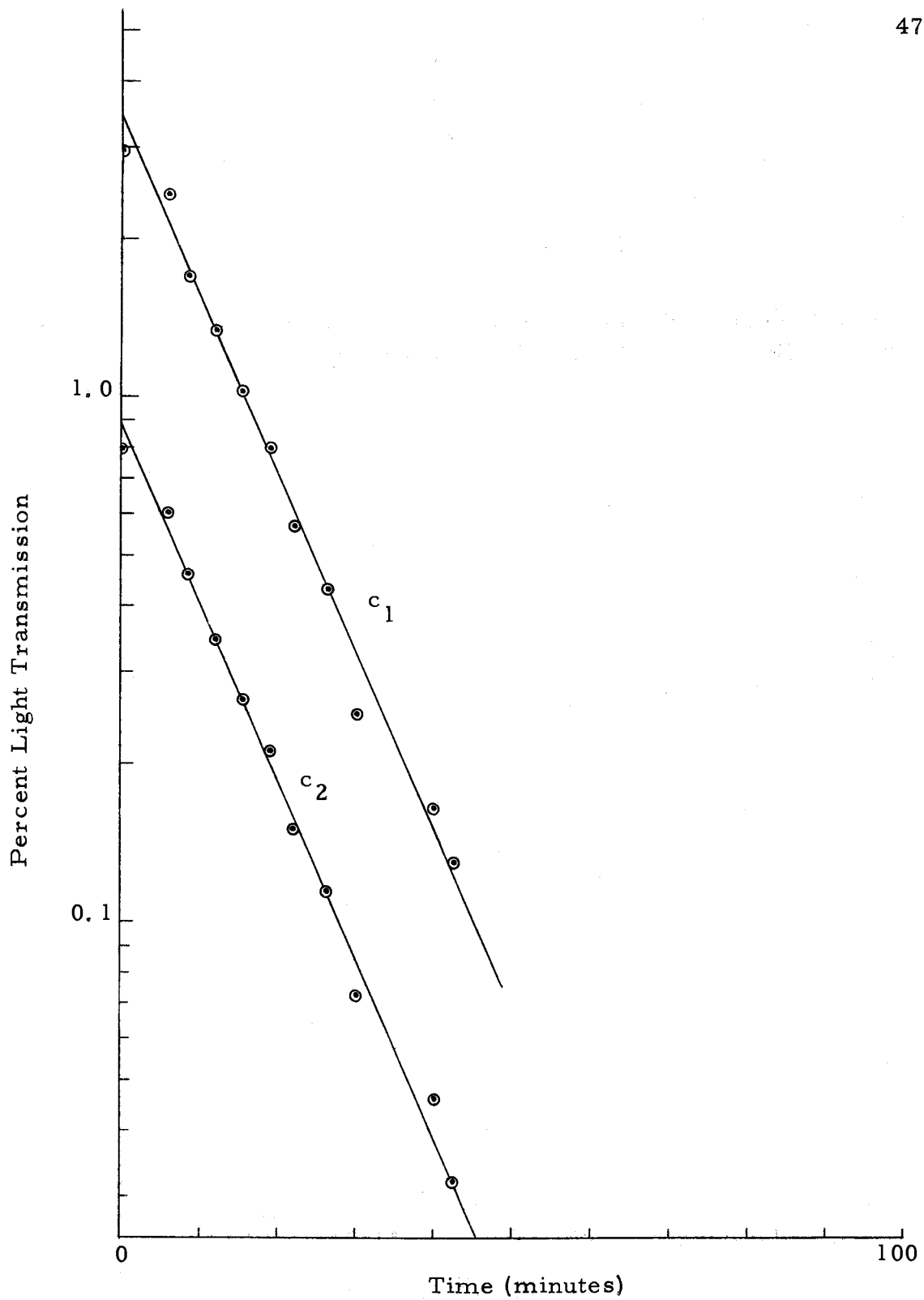


Figure 17. Percent Light Scatter vs. Time for Challenging Aerosol, c_1 and Penetrating Aerosol, c_2 . $h = 4$, $V_o = 25.00$ ft/min.

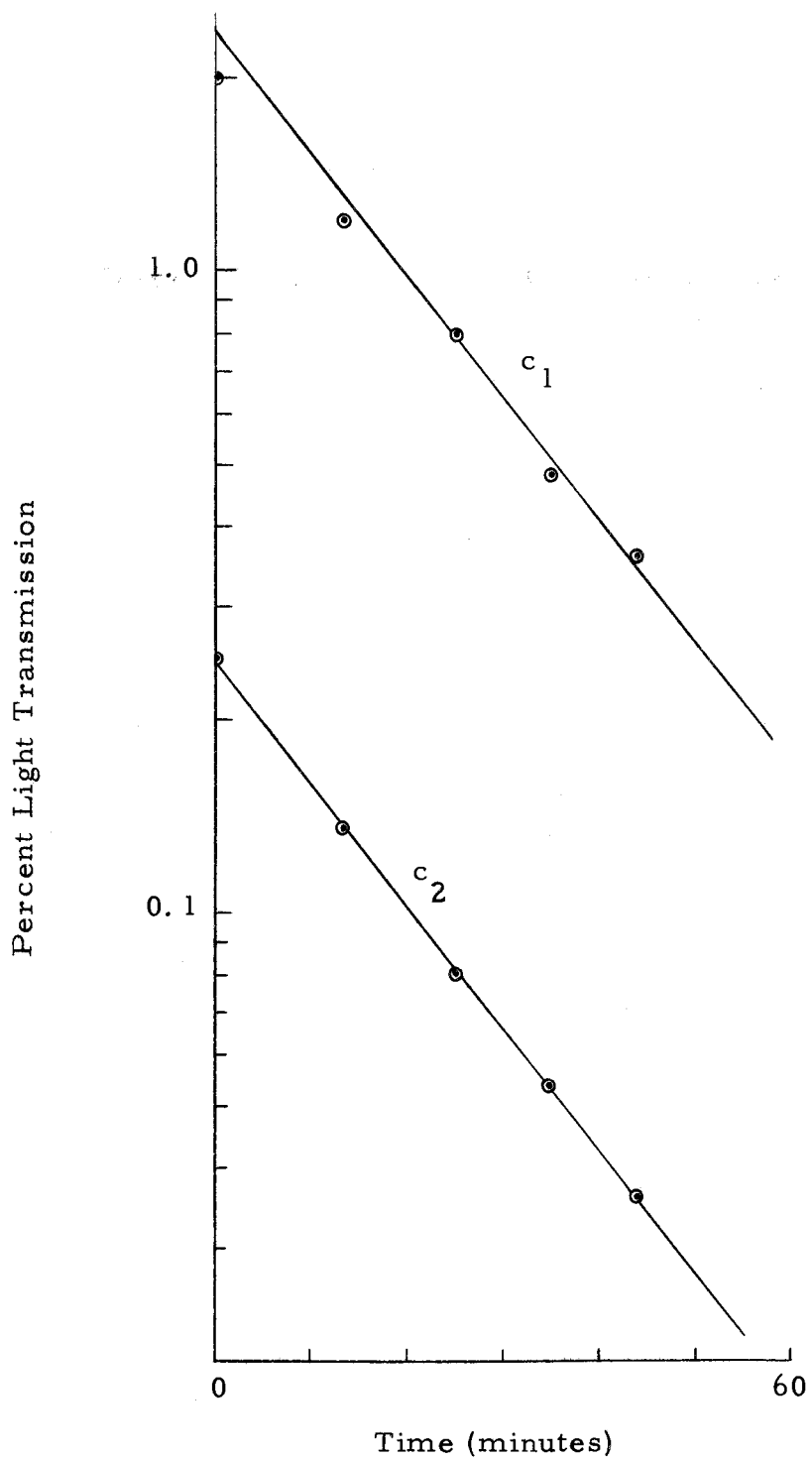


Figure 18. Percent Light Scatter vs. Time for Challenging Aerosol, c_1 and Penetrating Aerosol, c_2 . $h = 6$, $V_o = 8.75$ ft/min.

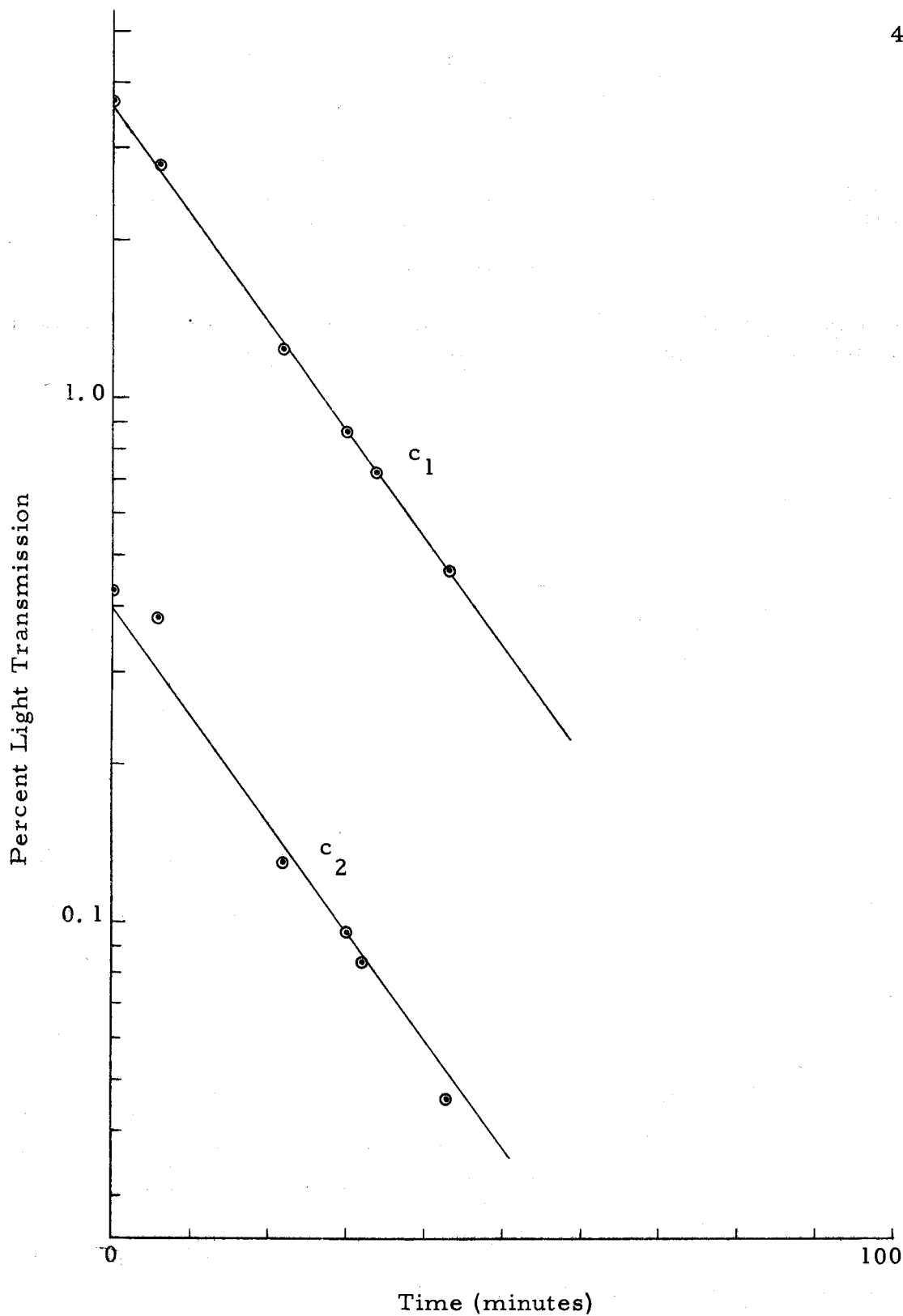


Figure 19. Percent Light Scatter vs. Time for Challenging Aerosol, c_1 and Penetrating Aerosol, c_2 . $h = 6$, $V_o = 10.96$ ft/min.

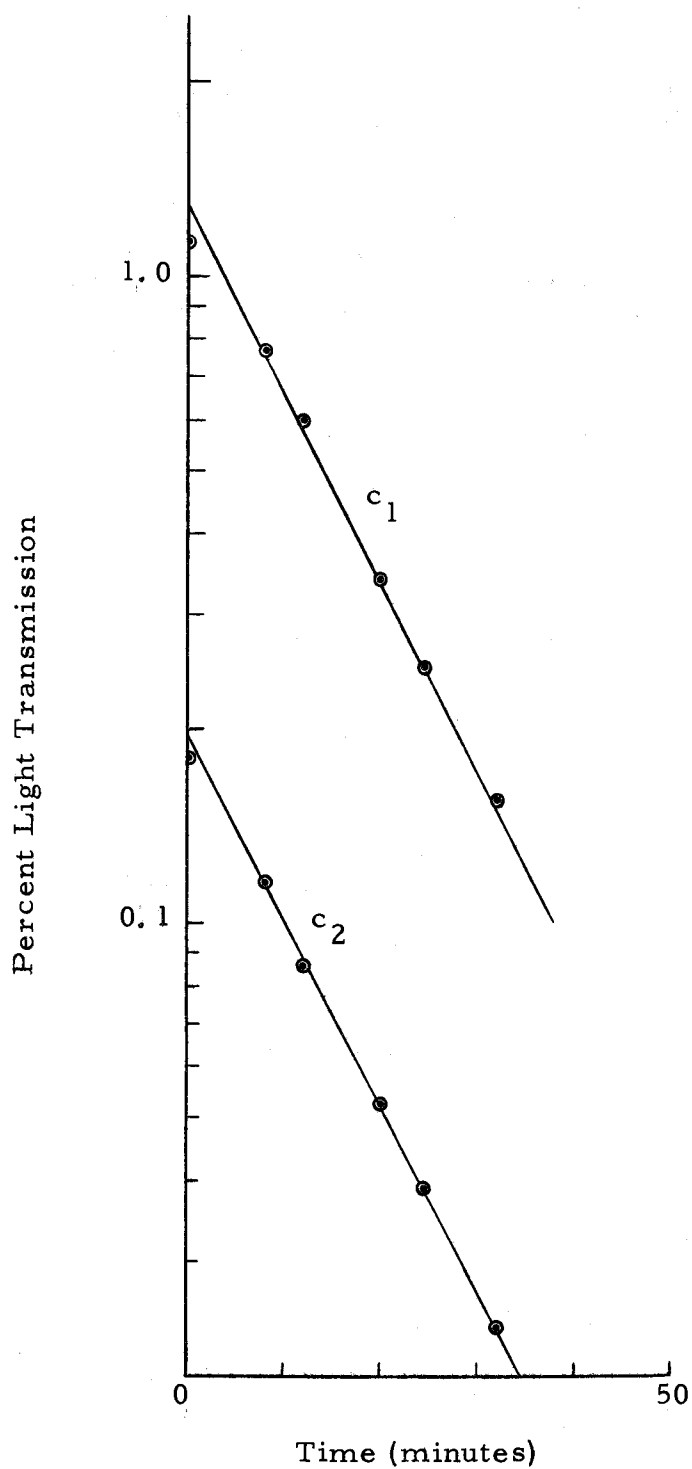


Figure 20. Percent Light Scatter vs. Time for Challenging Aerosol, c_1 and Penetrating Aerosol, c_2 . $h = 6$, $V_o = 14.65$ ft/min.

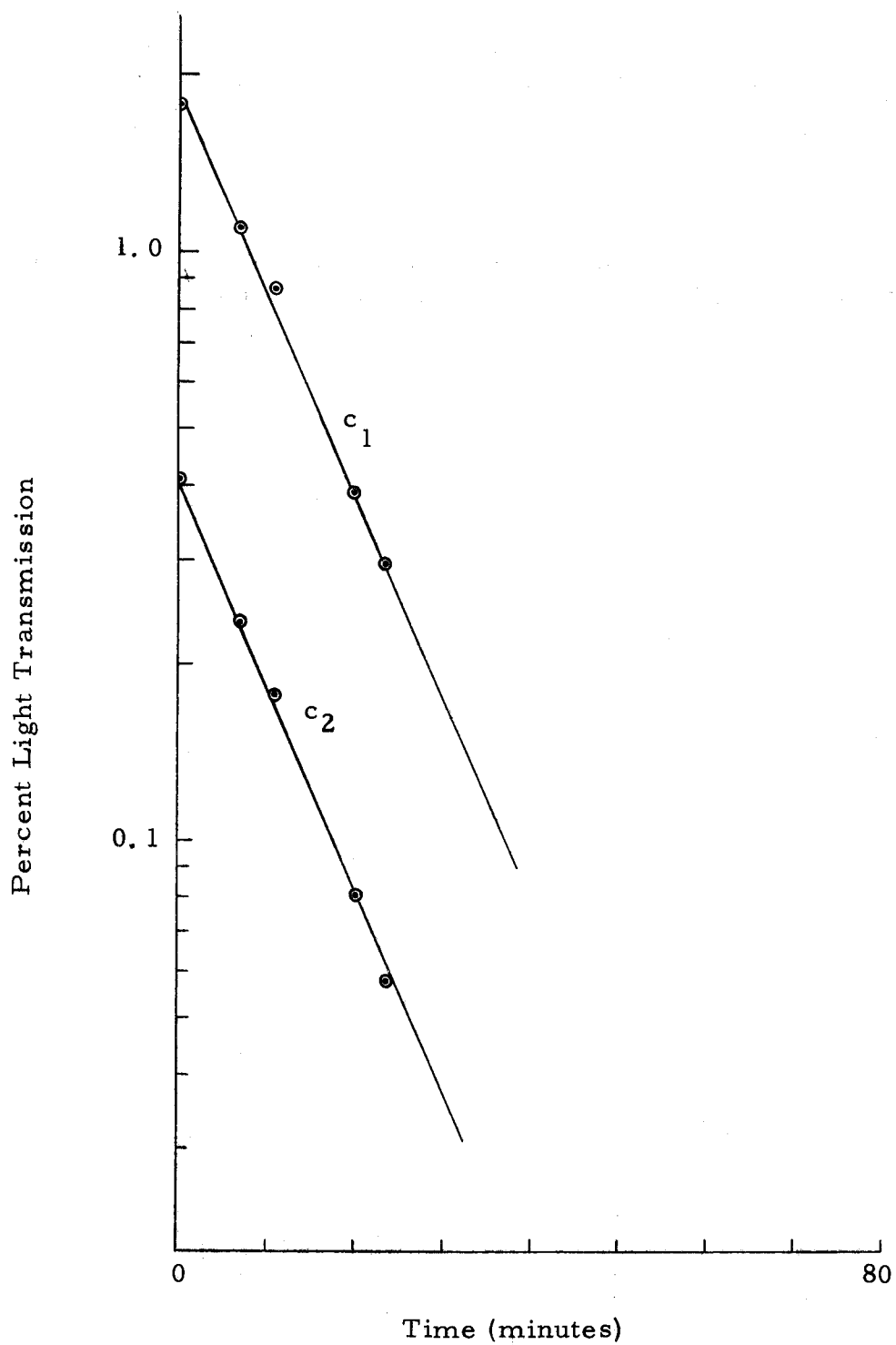


Figure 21. Percent Light Scatter vs. Time for Challenging Aerosol, c_1 and Penetrating Aerosol, c_2 . $h = 6$, $V_0 = 25.00$ ft/min.

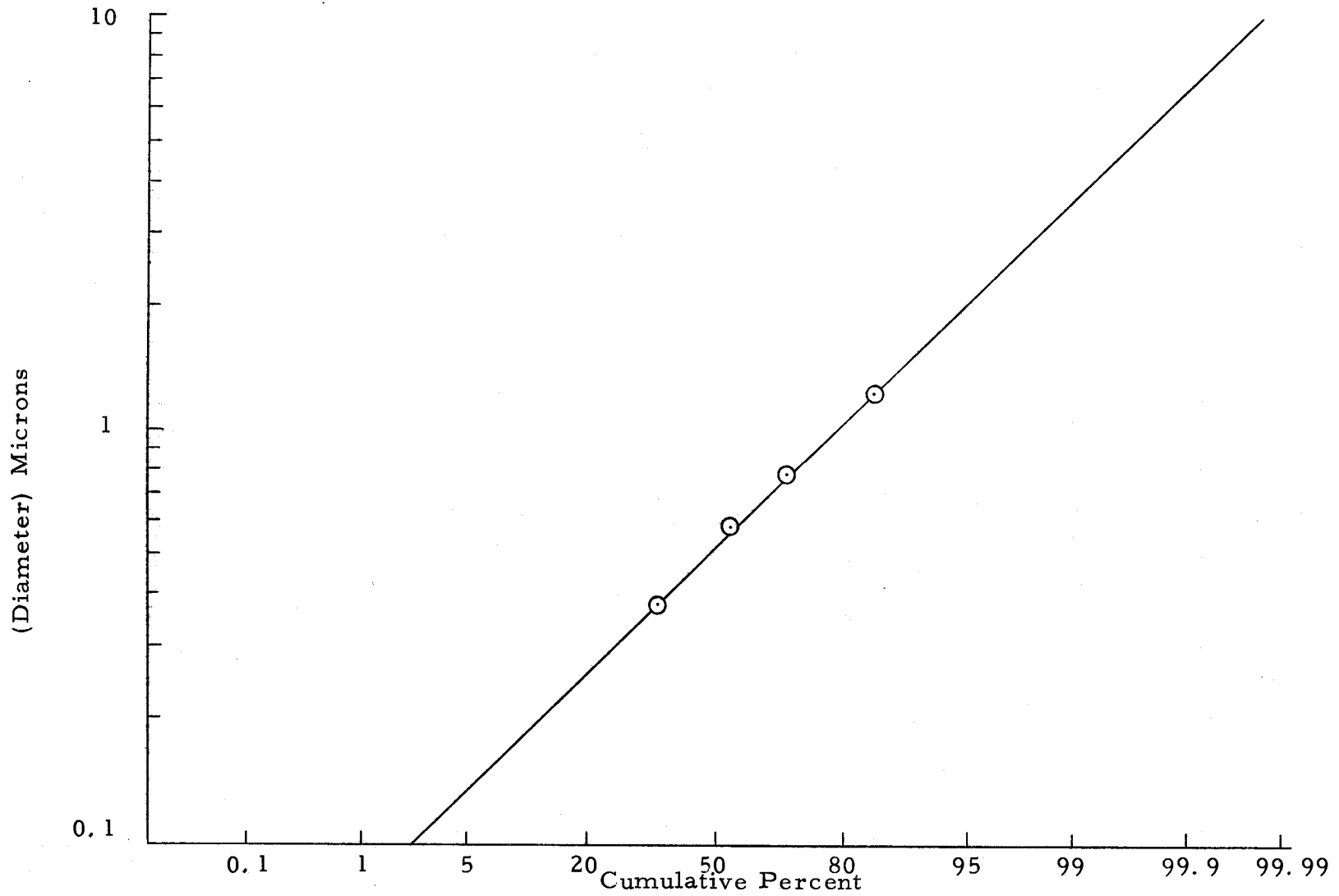


Figure 22. Size Distribution of Challenging Aerosol (NH_4Cl), Logarithmic Probability Graph.

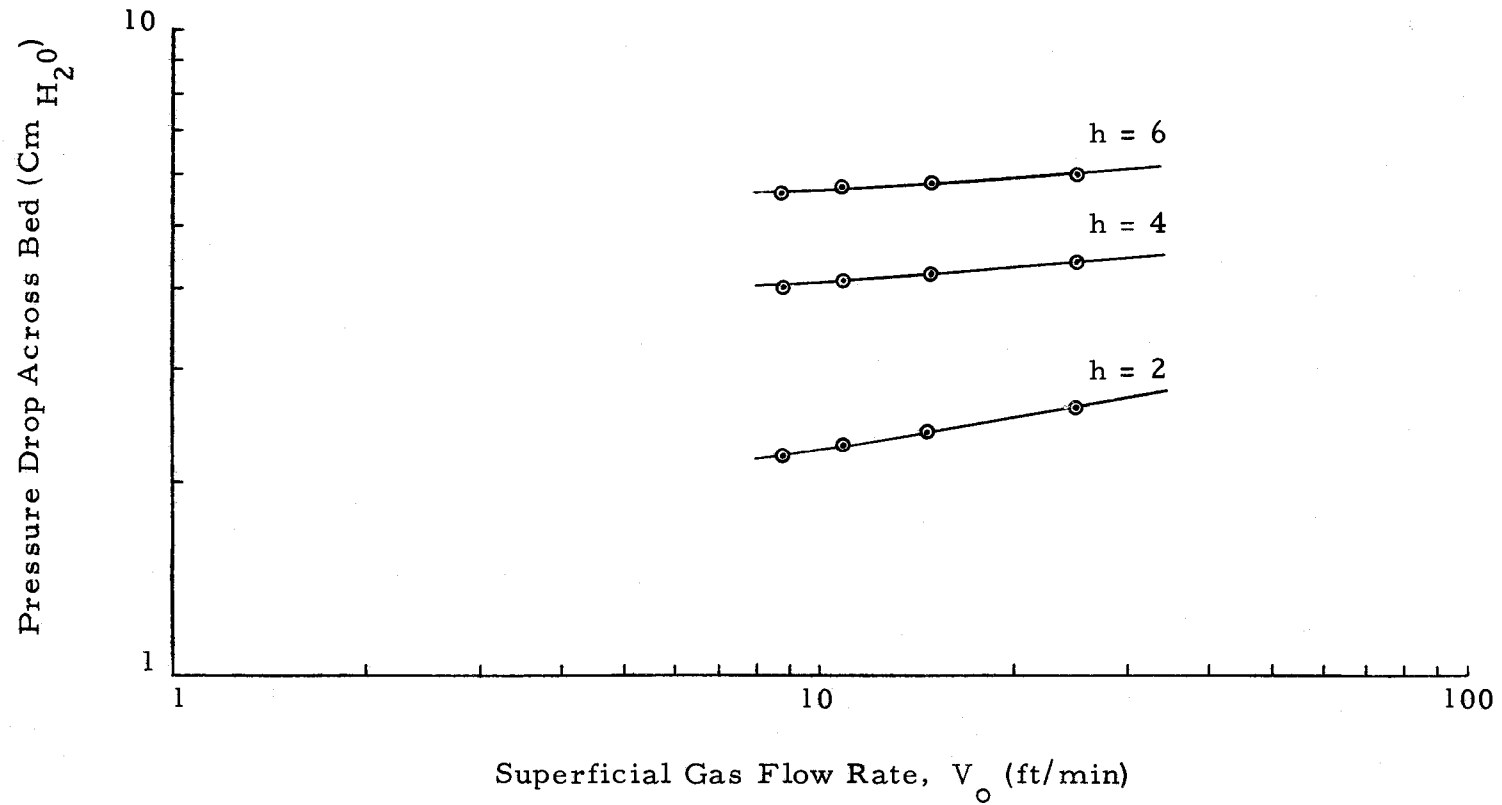


Figure 23. Results of Pressure Drop Measurements Across Fluidized Bed at Various Gas Flow Rates and Bed Heights.

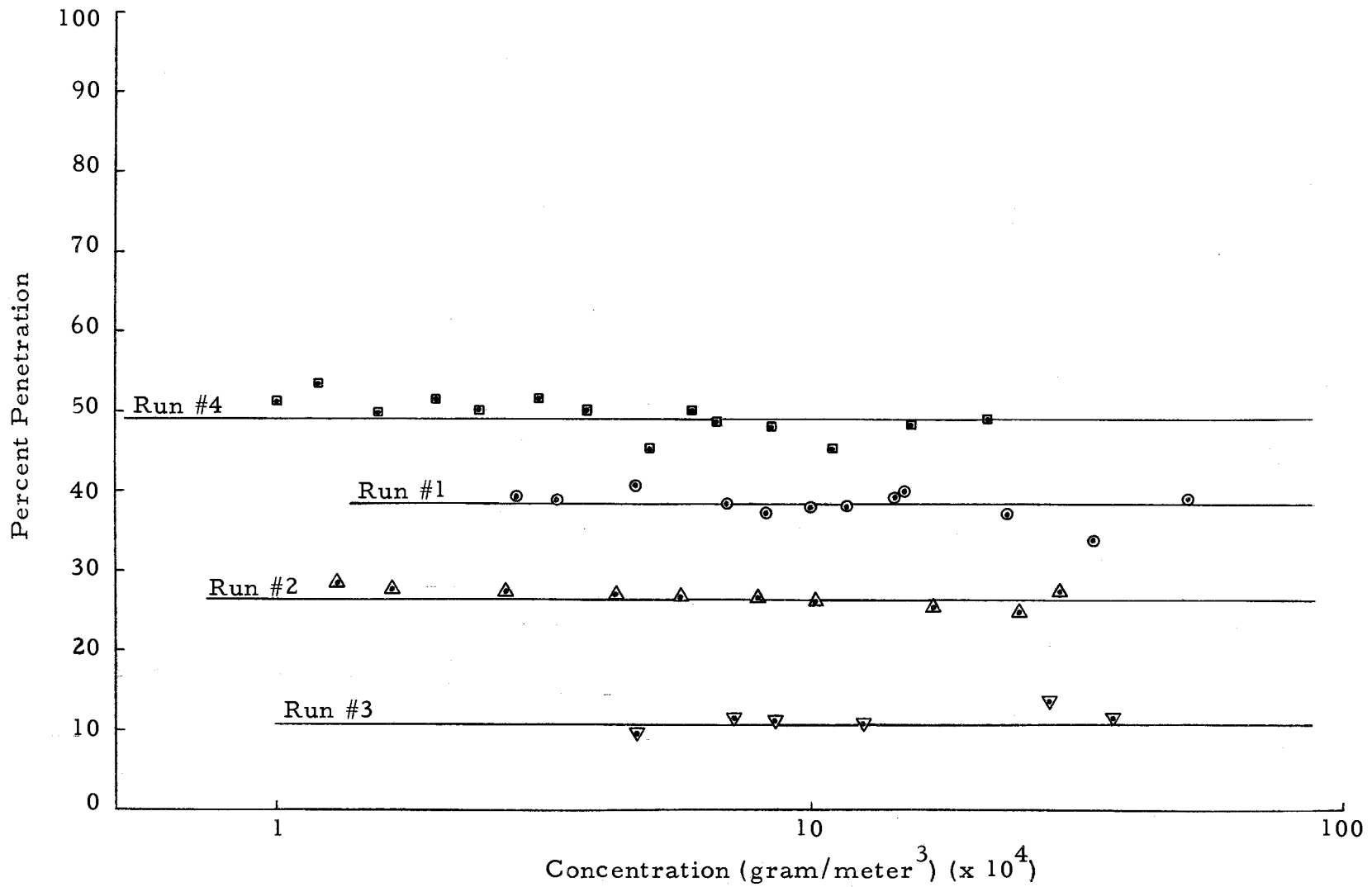


Figure 24. Results of Fluidized Bed Filtration Efficiency Measurements for Different Levels of Challenging Aerosol Concentration.

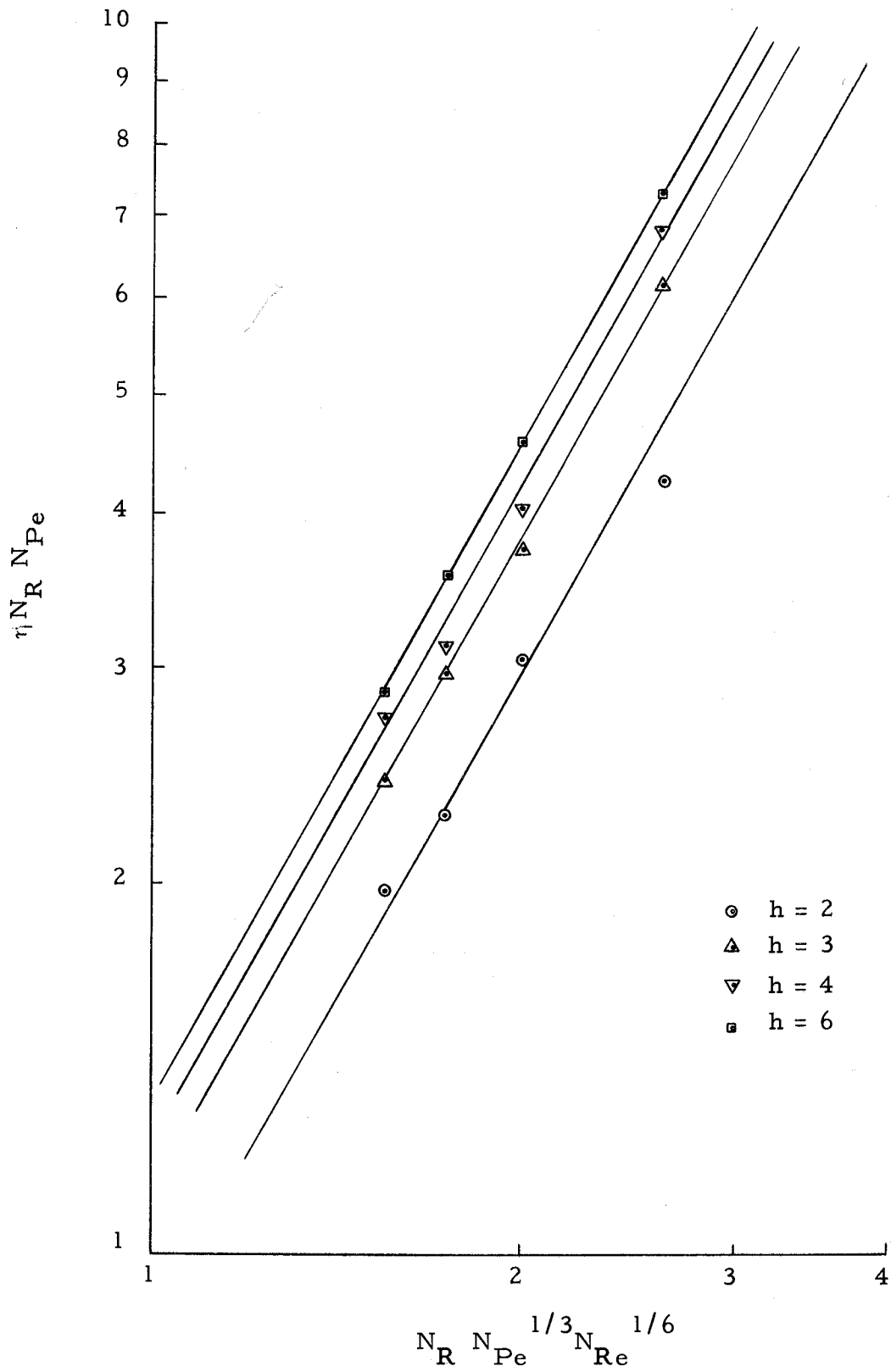


Figure 25. Recalculated Data showing Single Valued Functions with Slope of 1.78.

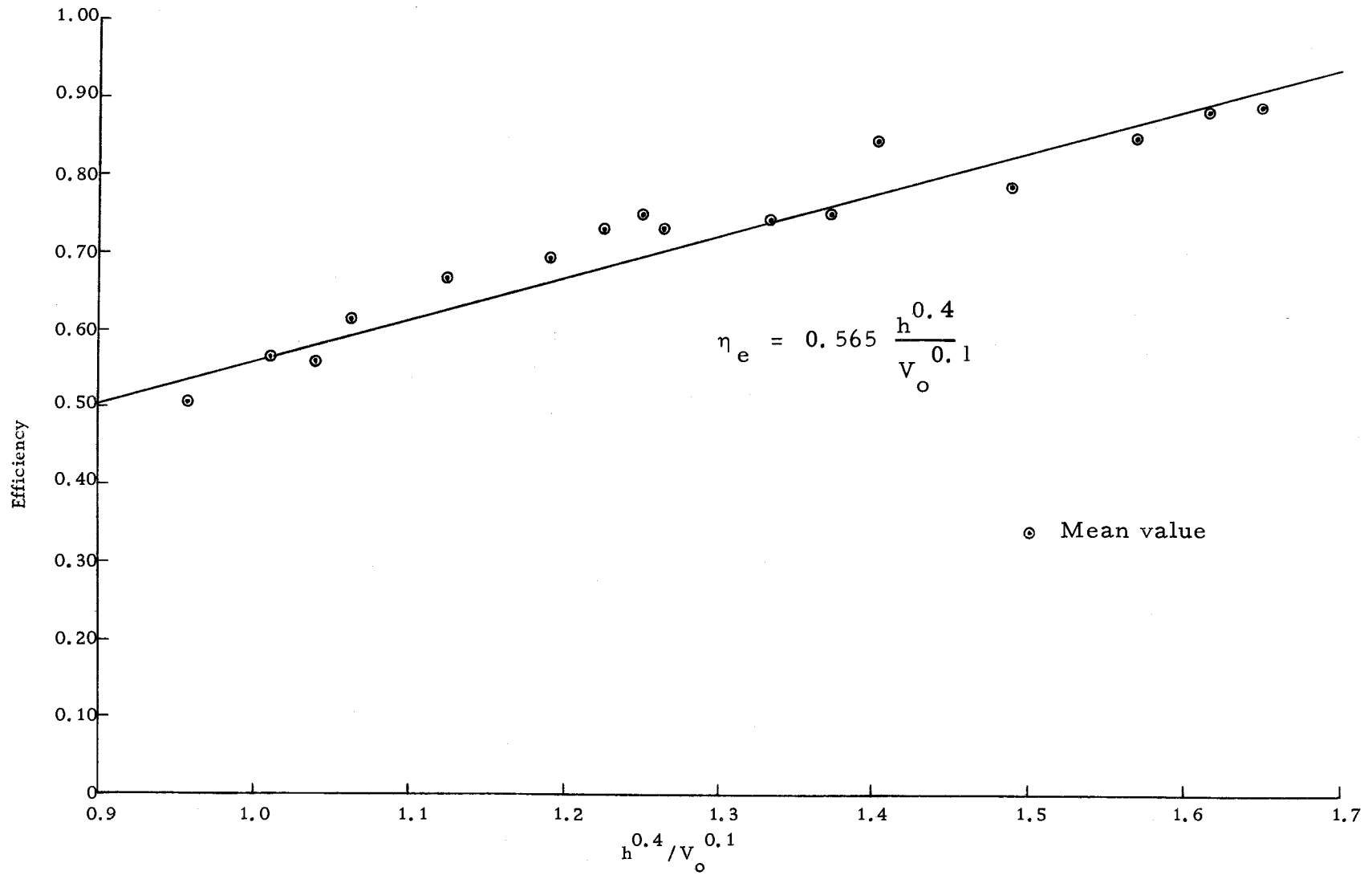


Figure 26. Efficiency Data and Curve Representing Equation 28.

CONCLUSIONS

Referring to equation (19), it is to be expected that as the height-to-diameter ratio of the fluidized bed, h , was increased, efficiency would increase. As will be shown later, the bed height resulted in an exponential decay of the penetrating aerosol as in the following relationship.

$$- \ln (1 - \eta) \approx h \quad (20)$$

The fact that gas flow rate appears in the denominator of equation (19) offers some interesting aspects of the mechanisms of filtration by the fluidized bed. If the filtration mechanism is presumed to be inertial impaction between ammonium chloride particles and bed particles, an equation can be derived by a simple treatment based on this mechanism.

Assuming impaction likelihood varies with the total number of collisions present in a given system, and N is the number of collisions per unit volume per unit time, then it is clear that N will be a function of c , the aerosol concentration, and $\beta \rho_f$, the bed concentration. It is further evident that N must be proportional to dc/dt , the rate of change of aerosol concentration with time. The following equation, therefore, applies to a horizontal slice of gas of differential thickness travelling with a velocity V_o , up through a bed of fluidized particles.

$$-\frac{dc}{dt} = K' c \rho_f \beta \quad (21)$$

For a given aerosol-bed system, K' is probably a function of size and shape of both bed material and aerosol in addition to average kinetic energy. Therefore, K' can be expressed as $K' = KV_o^2$. Furthermore, $V_o dt = dh$. Making appropriate substitutions and integrating, results in the following expression

$$-\ln \frac{c_2}{c_1} = KV_o^2 \rho_f \beta h \quad (22)$$

or that

$$\eta_e = 1 - e^{-K\rho_f \beta h} \quad (23)$$

This is, in fact, essentially the relationship that Meissner and Mickley found to apply to a fluidized bed filtration system. However, it does not apply in the present study. The basic difference between the two studies is that the average particulate mass used in the present study is two to three orders of magnitude smaller than that used in Meissner and Mickley's work. Therefore, inertial forces in the present study would be much smaller. In Meissner and Mickley's work, inertial impaction was undoubtedly the predominant filtration mechanism, but in the present study, the data indicate that inertial impaction was not the major contributor to filtration of the aerosol.

Figures 27a and 27b show photomicrographs (1000X) of bed

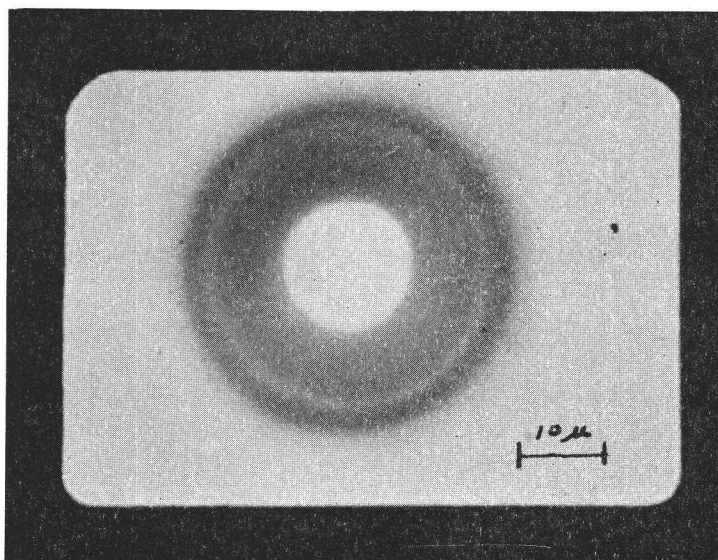


Figure 27a. Photomicrograph (1000X) of Bed Material before Being used as Filtration Media. Dark Ring is Part of Glass Shot out of Depth of Focusing Field.

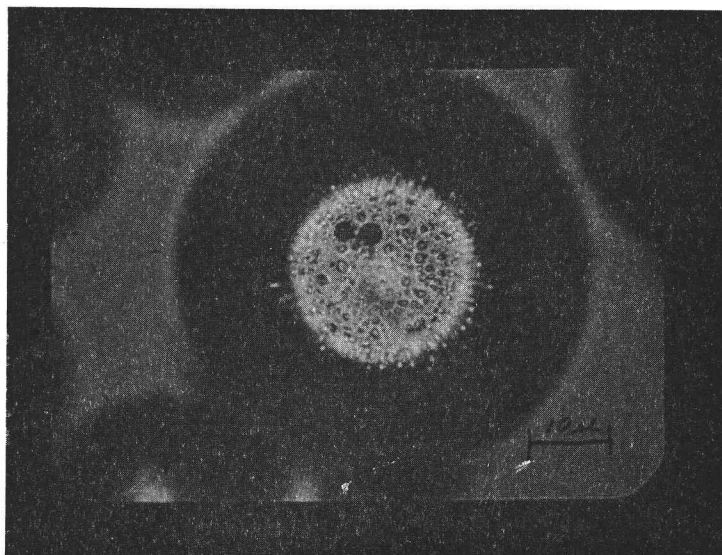


Figure 27b. Photomicrograph (1000X) of Bed Material after being used as Filtration Media.

material before and after being used as filter media. The aerosol is clearly shown collected upon the bed material. The question arises-- If impaction is not the major filtration mechanism, then by what means did the bed material remove the aerosol from the air stream?

Evaluation of each of the pertinent theoretical target efficiencies was made to determine which filtration mechanisms were effective in the present study. These parameters and values for estimated target efficiencies are listed in Table II. Of these parameters, only the interceptive mechanism shows "strong" target efficiencies for this study. However, it was felt that other filtration mechanisms were operative as the interceptive mechanism is independent of velocity and efficiencies in the study showed a slight velocity effect. Furthermore, as noted before, interception never occurs alone, but always as a limiting case of another form of filtration.

Table II. Filtration Mechanism Parametric Values and Calculated Target Efficiencies

Parameter	Parameter Value	Efficiency, η	Equation
N_R (Interception)	2×10^{-2}	.83	(4)
N_I (Inertial Impaction)	4×10^{-3}	0	
N_{Pe} (Browning Diffusion)	2×10^3	.063	(7)
K_I (Induced Electrostatic Attraction)	2×10^{-4}	.088	(10)
K_E (Charged Particles Electrostatic Attraction)	3×10^{-3}	.0094	(11)

It will be noted that the inertial impaction parameter is 0.004. This is far below the critical value for N_I , which theory states corresponds to the minimum particle size, below which impaction cannot take place (1). Therefore, it is assumed that any filtration in the system under study by inertial impaction may be considered negligible.

Reference 1 notes that the most satisfactory quantitative correlation of effective filter efficiency, η_e , with the combined effects of Brownian diffusion and interception is that proposed by Friedlander (9). Assuming Lamb's solution for viscous flow for values of $N_I \ll 1$, the following relationship was suggested

$$\eta_e N_R N_{Pe} = 6(N_R N_{Pe}^{1/3} N_{Re}^{1/6}) + 3(N_R N_{Pe}^{1/3} N_{Re}^{1/6})^3 \quad (24)$$

It will be noted that as $N_R \rightarrow 0$ (pure diffusion) the second term goes to zero and as $N_{Pe} \rightarrow \infty$ (pure interception) the first term goes to zero. Reference 1 cites extensive data taken from Chen, Ranz and Wong (19) and others covering ranges of $5(10^{-4}) < N_I < 1$ and $N_{Re} < 1$ confirm Friedlander's proposal and could be fitted to equation (24).

Equation (24) also predicts a minimum efficiency for a certain particle size. This may be found by substituting the definitions for the dimensionless groups, differentiating with respect to D_p ,

and equating to zero. The result is

$$D_{P_{\min}} = 0.488 \frac{(kT)^{1/4}}{(\mu \rho)^{1/8}} \left(\frac{D_f}{V_o}\right)^{3/8} \quad (25)$$

This represents the particle size corresponding to minimum efficiency for a filtration system utilizing Brownian diffusion and interception as filtration mechanisms. The existence of the minimum is established because $d^2 \eta_e / dD_p^2$ is always positive. Figure 28 indicates a series of curves corresponding to different gas flow rates when effective filter efficiencies, η_e , are plotted against particle size, D_p , according to equation (24). Viscosity of gas, μ , was taken to be 181.2 poises and density (ρ) to be 0.0818 Lb_m/Ft^3 .

A series of measurements were made to determine the size of particulate most difficult to filter by use of the fluidized bed. This analysis (see Appendix A) demonstrated, as shown in Figure 29, that minimum filtration efficiency was encountered when the challenging aerosol diameter was approximately 0.5 microns when the superficial gas velocity was 14 feet per minute. It is noted that the mean size of the aerosol used in this study was close to the size most difficult to filter.

Dimensionless parameters from the data were determined and efficiency values of the fluidized bed were used in plotting $\eta_e N_R N_{Pe}$ vs. $N_R N_{Pe}^{1/3} N_{Re}^{1/6}$. Data for the various bed height-to-

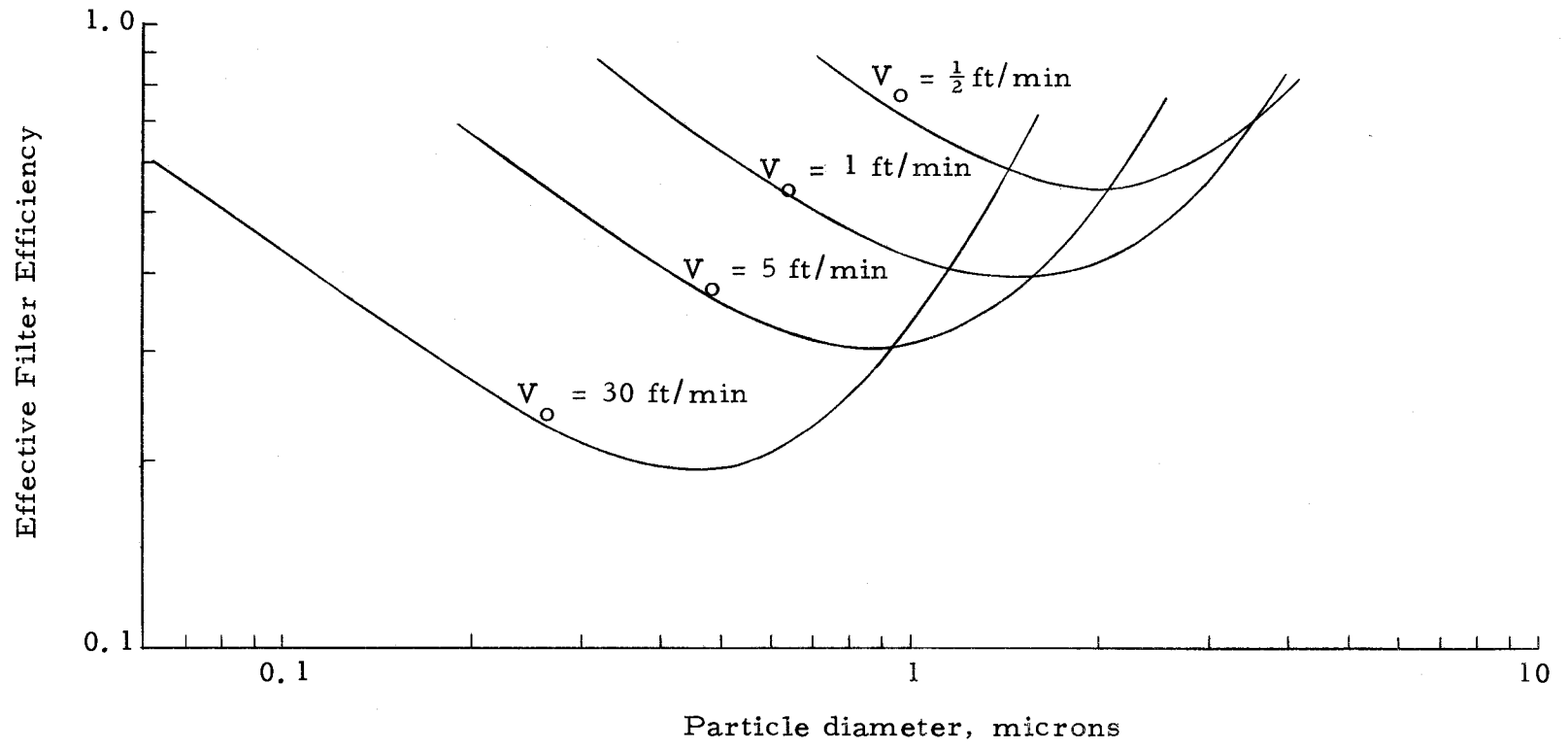


Figure 28. Effective Filter Efficiency vs. Particle Size for Different Flow Rates. Filtration Mechanisms are Browning Diffusion and Interception.

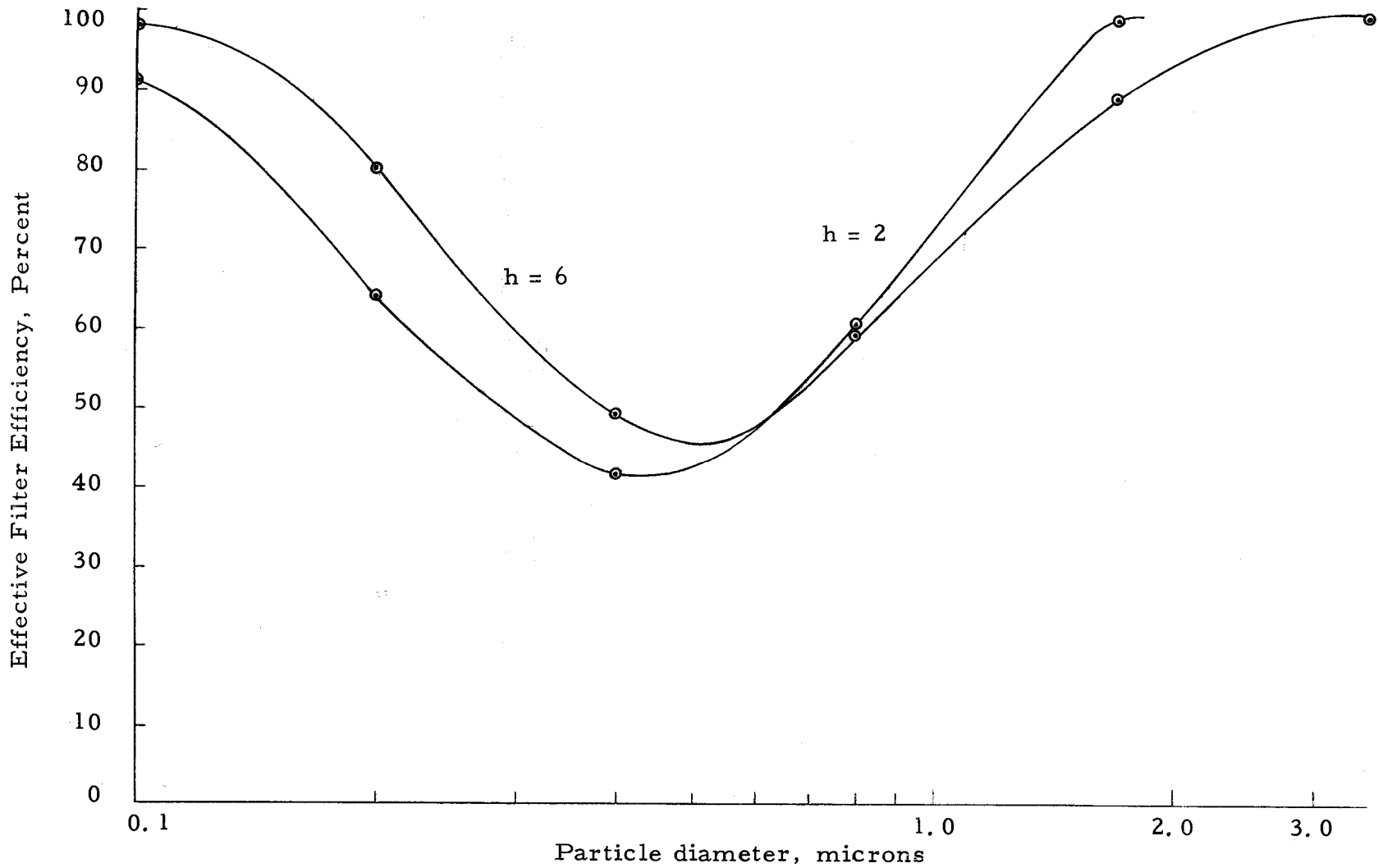


Figure 29. Fluidized Bed Effective Filter Efficiency vs. Challenging Aerosol Particles Size for Various Bed Height-to-Diameter Ratios, h . Superficial gas velocity equals 14 ft/min.

diameter ratio h , used in the present study plotted as straight lines, as shown in Figure 25. The spacing between the lines can be related by the following equation

$$- \text{Ln} \frac{c_2}{c_1} = Kh \quad (26)$$

This is the exponential decay factor for the penetrating aerosol mentioned above.

The curves in Figure 25 can be represented in the following form

$$\eta_e = \frac{(N_{Pe}^{1/3} N_{Re}^{1/6} N_R)^{1.78} (h)^{0.4} 5.1 \times 10^4}{(N_R N_{Pe})} \quad (27)$$

By using the definition for the dimensionless parameters and substituting appropriate values for those factors that remained constant in the present study, equation (27) may be expressed in terms of the independent variables.

$$\eta_e = 0.565 \frac{h^{0.4}}{V_o^{0.1}} \quad (28)$$

It will be noted in equation (24) that the slope of the curve for pure diffusion is one while the slope of the curve for pure interception is three. The fact that the slope of the lines in Figure 25 is

between one and three implies both Brownian diffusive and interceptive forces are active in the fluidized bed under consideration. Noting that the operating conditions are close to that for minimum efficiencies (see Figure 28) substantiates that both forces are active. Friedlander (9) pointed out that the intercept of the lines (Figure 25) are probably dependent on filter porosity and distribution.

Target efficiencies for interaction between a charged particle and charged collector based on equation (11) were considered too low to be considered significant, even when assuming the particle to have as high a charge as one electron each. However, target efficiency based on the interaction between a charged collector and a dielectric particle on which the collector induces a charge (equation 10) was of the same order of magnitude as target efficiencies based upon Brownian diffusion. The value determined for K_I was based upon a maximum charge density of 2.65×10^{-9} coulombs per square centimeter for charged surfaces in air. Higher charges would leak away through air ionization and corona discharge. Air ionization and corona effects were frequently observed during the operation of the fluidized bed. The dielectric constant for ammonium chloride was taken as 6.8.

Redefining target efficiency for induced electrostatic attraction, equation (10), in terms of the Peclet number results in

$$\eta_e = KN_{Pe}^{1/2.5} \quad (29)$$

For the range of Peclet numbers in the present study, changing the exponent to 1/3, for approximation purposes, resulted in errors of only about three percent. Assuming induced electrostatic attraction operates in the same manner as Brownian diffusion, the effects of induced electrostatic attraction would not change the slope of curves in Figure 25 appreciably. However, the intercept would be affected. Therefore, the constant in Equation 19 probably reflects induced electrostatic attraction in addition to bed porosity and distribution. This is in agreement with Friedlander's (8) suggestion that electrical effects might result in enhanced efficiency. At the present time, there is no method of analysis to determine the relative affects of electrostatic attraction and Brownian diffusion.

It was noted that very little reentrainment of the particulate was found during the tests of the fluidized bed. It is assumed that electrostatic attraction was probably the major force holding the particles to the bed material.

Knowing the effect of the variable of equation (27), optimization of collection efficiency may be realized for the fluidized bed when $N_{Re} < 1$ and $N_I \ll 1$. Substituting definitions for dimensionless parameters in equation (27), we have

$$\eta_e = 5.1 \times 10^4 \left(\frac{hCkT}{3\pi} \right)^{0.4} \frac{D_p^{1.15} \rho^{0.30}}{D_f^{1.67} \mu^{0.71} V_o^{0.1}} \quad (29)$$

Note that the Cunningham correction factor, C , is a function of particle diameter, D_p . Any analysis of the effect of changing particle size requires appropriate changes to the Cunningham correction factor. The constant is considered to be a function of electrostatic attraction, and bed porosity and distribution. Changes to bed material size, D_f , may affect the value of this constant.

In summary, the fluidized bed investigated can provide efficiencies of filtration on a count basis of over 90 percent for sub-micron particulate. It is interesting to note that the pressure drop across the filtration system does not change radically with changes in gas velocity, and that changes in gas velocity do not have appreciable affect on filtration efficiencies. This is not true with many filtration systems. Thus, a fluidized bed, by maintaining moving elements in proper position with respect to each other and the gas stream containing an aerosol, offers an effective filtration media for submicron particulate and the opportunity to be regenerated on a continuous basis without shut-down of the system.

BIBLIOGRAPHY

1. American Petroleum Institute. Removal of particulate matter from gaseous wastes, filtration. New York, 1961. 56 p.
2. American Petroleum Institute. Removal of particulate matter from gaseous wastes, wet collectors. New York, 1961. 47 p.
3. Chakravarty, R. K. et al. Application of fluidized technique in gas purification. Indian Journal of Technology 1:423-426. 1963.
4. Dimmick, Robert L., Melvin T. Hatch and James Ng. A particle-sizing method for aerosols and fine powders. Archives of Industrial Health 18:23-29. 1958.
5. Frantz, Joseph F. Design for fluidization, part 1. Chemical Engineering 69:161-178. September 17, 1962.
6. Frantz, Joseph F. Design for fluidization, part 3. Chemical Engineering 69:103-110. October 29, 1962.
7. Friedlander, S. K. Mass and heat transfer to single spheres and cylinders at low Reynolds numbers. A. I. Ch. E. Journal 3: 43-48. March, 1957.
8. Friedlander, S. K. Particle diffusion in low speed flows. Paper presented at the 59th Annual Meeting of the Air Pollution Control Association, San Francisco, 1966. 17 p. (Paper no. 66-83) (Processed)
9. Friedlander, S. K. Theory of aerosol filtration. Industrial and Engineering Chemistry 50:1161-1164. 1958.
10. Gillespie, T. The role of electric forces in the filtration of aerosols by fiber filters. Journal of Colloid Sciences 10:299-313. 1955.
11. Hatch, Theodore. Determination of "average particle size" from the screen analysis of non-uniform particulate substances. Journal of the Franklin Institute 215:27-37. 1957.
12. Hayakawa, Ichiya. The effects of humidity on the coagulation rate of ammonium chloride aerosols. Journal of the Air Pollution Control Association 14:339-346. 1964.

13. Johnstone, H. F., R. B. Field and M. C. Tassler. Gas absorption and aerosol collection in a venturi atomizer. *Industrial and Engineering Chemistry* 46:1601-1608. 1954.
14. Kraemer, Herber F. and H. G. Johnstone. Collection of aerosol particles and in presence of electrostatic fields. *Industrial and Engineering Chemistry* 47:2426-2434. 1965.
15. Landahl, H. D. and R. G. Hermann. Sampling of liquid aerosols by wires, cylinders and slides, and efficiency of impaction of the droplets. *Journal of Colloid Science* 4:103-136. 1949.
16. Leva, Max. Flow behavior in fluidized systems. *Chemical Engineering* 64:289-293. October, 1957.
17. Leva, Max. *Fluidization*. New York, McGraw-Hill, 1959. 327 p.
18. Meissner, H. P. and H. S. Mickley. Removal of mists and dusts from air by beds of fluidized solids. *Industrial and Engineering Chemistry* 41:1238-1242. 1949.
19. Ranz, W. E. and J. B. Wong. Impaction of dust and smoke particle. *Industrial and Engineering Chemistry* 6:1371-1381. 1952.
20. Silverman, Leslie. Performance of industrial aerosol filters. *Chemical Engineering Progress* 47:462-467. 1951.
21. Stairmand, C. J. Dust collection by impingment and diffusion. *Transactions of Institution of Chemical Engineers (London)* 28: 130-139. 1950.
22. Wong, J. B., W. E. Ranz and H. F. Johnstone. Inertial impaction of aerosol particles on cylinders. *Journal of Applied Physics* 26:244-249. 1955.

APPENDICES

APPENDIX A

STATISTICAL METHOD FOR FILTER EVALUATION

In the present study, it was desired to obtain the efficiency of filtration as a function of particle size similar to that obtained by the Fractional Particle Size-Efficiency Air Filter Test. However, the objections of greater number of evaluations required and limitations of controlling particulate size precluded the use of that test. To this end, the following technique was developed. That is, a system was devised whereby filtration efficiency as a function of particle size could be determined as a result of challenging the system only once and without having to control the size of the challenging aerosol.

All particles are assumed spherical and are measured as their equivalent spherical diameter. This is quite valid for particles such as ammonium chloride generated by sublimation and subsequent condensation. Furthermore, it is assumed that all particles are homogeneous and have the same density.

By definition, the effective filter efficiency is

$$\eta_e = \left[1 - \frac{P_2}{P_1} \right] 100 \quad (30)$$

where P_1 and P_2 are the total number of particles challenging and penetrating the filter system. Then for particles of "i"

size

$$\eta_{e_i} = \left[1 - \frac{P_{i_2}}{P_{i_1}} \right] 100 \quad (31)$$

where "i" describes particles of "i" size only. If the samples S_1 and S_2 are truly representative of P_1 and P_2 , then

$$\frac{S_i}{S} = \frac{P_i}{P} \quad (32)$$

If the particles are homogeneous and spherical, with a mean size with respect to mass, D_m , then

$$W = P \left(\frac{\pi \rho_p}{6} \right) D_m^3 \quad (33)$$

where W is the total weight of particle population. Combining (32) and (33)

$$P_i = \frac{S_i}{S} \left(\frac{6W}{\pi \rho_p D_m^3} \right) \quad (34)$$

Then for condition, "1"

$$P_{i_1} = \left(\frac{S_i}{S} \right)_1 \frac{6W_1}{\pi \rho_p D_{m_1}^3} \quad (35)$$

and condition "2"

$$P_{i_2} = \left(\frac{S_i}{S}\right)_2 \frac{6W_2}{\pi \rho_p D_{m_2}^3} \quad (36)$$

Substituting (35) and (36) into (31)

$$\eta_i = 1 - \frac{\left(\frac{S_i}{S}\right)_2 \left(\frac{6W_2}{\pi \rho_p D_{m_2}^3}\right)}{\left(\frac{S_i}{S}\right)_1 \left(\frac{6W_1}{\pi \rho_p D_{m_1}^3}\right)} 100 \quad (37)$$

Cancelling like terms and rearranging,

$$\eta_i = \left[1 - \frac{\left(\frac{S_i}{S}\right)_2}{\left(\frac{S_i}{S}\right)_1} \left(\frac{W_2}{W_1}\right) \left(\frac{D_{m_1}}{D_{m_2}}\right)^3 \right] 100 \quad (38)$$

Hatch has noted that if the basic distribution by count is log-normal with mean D_m and geometric deviation σ_g , then the j th moment distribution ($j = 2$ for distribution of surface area; $j = 3$ for that of particulate volume) is again log-normal with the same geometric deviation σ_g and with means related by

$$\text{Ln } D_j = \text{Ln } D_p + j \text{Ln}^2 \sigma_g \quad (39)$$

or

$$\text{Ln } D_m = \text{Ln } D_p + 3 \text{ Ln}^2 \sigma_g \quad (40)$$

A log-normal distribution of particles with respect to size appears as a straight line when plotted on log-normal probability paper, as shown in Figure (22). The mean size with respect to number (D_p) is that size where the line crosses the 50% value. The geometric deviation of the distribution is given by the ratio of the 84% value divided by the 50% value of the size. Using these values in equation (40), the ratio

$$\frac{D_{m_1}}{D_{m_2}}$$

may be computed for the particulate distribution.

Values of S_1/S may be obtained from Table II by using cumulative percentage values from a logarithmic probability graph of the size distribution. Weights W_1 and W_2 may be obtained in any standard manner.

Measurements were made of the size distribution of challenging and penetrating aerosols for a fluidized bed with a superficial gas velocity of 14.0 feet per minute. The foregoing analysis was applied to these distributions. Figure 29 shows the effective filtration

Table III. Ordinate and Cumulative Percent Values for Normal Distribution

Cumulative Percent	$\frac{Si}{S}$	Cumulative Percent
0.001	0.00007	99.999
0.01	0.0007	99.99
0.1	0.0040	99.9
0.5	0.0145	99.5
1.0	0.0262	99.0
2.0	0.0484	98.0
2.5	0.0585	97.5
3.0	0.0691	97.0
4.0	0.0862	96.0
5.0	0.1032	95.0
6.0	0.1191	94.0
7.0	0.135	93.0
8.0	0.151	92.0
9.0	0.162	91.0
10.0	0.175	90.0
15.0	0.233	85.0
20.0	0.280	80.0
25.0	0.317	75.0
30.0	0.347	70.0
35.0	0.370	65.0
40.0	0.387	60.0
45.0	0.395	55.0
50.0	0.399	50.0

efficiency of the fluidized bed as a function of particle size. Two curves are shown; one for bed height-to-diameter ratio of two and the other for bed height-to-diameter ratio of six.

Thus an efficiency curve for particulate size is available as a result of only one filter test and the size distribution analysis of challenging and penetrating aerosol populations. There is no need for controlling particulate size or for repeated tests.

APPENDIX B

NOMENCLATURE

- a = area of filter presented to gas stream, in square feet
- A = volume, liters
- c = aerosol concentration at time t, number per square foot
- c₀ = aerosol concentration at time zero, number per square foot
- c₁ = aerosol concentration of particles challenging filter or filter system (mass or number per unit volume of gas), in slugs or number per cubic foot
- c₂ = aerosol concentration of particles penetrating filter or filter system in slugs or number per cubic foot
- C = Cunningham correction factor to Stokes' law, for small particles, dimensionless:

$$C = 1 + \frac{2\lambda}{D_p} \left[1.23 + 0.41 \exp \left(-\frac{0.44D_p}{\lambda} \right) \right] \text{ for } 0.1 < \frac{2\lambda}{D_p} < 134$$

- D_{BM} = diffusivity due to Brownian movement = $\frac{CkT}{3\pi\mu D_p}$, in square feet per minute
- D_f = actual diameter of filter element in feet. (Assumed equal to mean size with respect to count)
- D_m = mean diameter of aerosol particle with respect to mass, in feet

D_p = mean diameter, with respect to count of aerosol particle, in feet

H = effective chamber height, feet

h = bed height-to-diameter ratio, dimensionless

k = Boltzmann's constant = $(1.380)(10^{-16})$ erg per deg k = $(5.65)(10^{-24})$ ft lb_f per deg R

K, K' = constants

$L_{1/2}$ = half life for concentration decay with time, minutes

N = total number of particles in a system

N_n = mean particle size with respect to number of particles, microns

N_m = mean particle size with respect to mass of particle, microns

P_1 = total number of particles challenging filtration system

P_2 = total number of particles penetrating filtration system

q_f = electrostatic charge on collector element, per unit area, in coulombs per square foot

q_p = electrostatic charge on aerosol particle, in coulombs

S_1 = total number of particles in a sample of P_1

S_2 = total number of particles in a sample of P_2

subscript i = refers to particles of " i " diameter only in one of the above

t = time, minutes

V_o = gas (and particle) approach velocity far upstream from

filtering element, in feet per minute

v = Stoke's settling velocity, feet per minute, for a given particle size and density

w = bed weight per unit area, pounds of solid per square foot

W_1 = total weight of P_1

W_2 = total weight of P_2

Dimensionless Groups

$$K_E = \frac{C q_f q_p}{3\pi\mu\epsilon_o D_p V_o}, \text{ parameter for coulombic attraction between}$$

particle and collector

$$K_I = \frac{2C(\epsilon_1 - \epsilon_2) q_f D_p^2}{18\mu\epsilon_o V_o D_f}, \text{ parameter for induced electrostatic}$$

charge on particle

$$N_I = \frac{4D_p^2 P C V_o}{3\mu D_f}, \text{ inertial impaction parameter}$$

$$N_{Pe} = \frac{V_o D_f}{D_{BM}}, \text{ Peclet number, Brownian diffusion parameter}$$

$$N_R = \frac{D_p}{D_f}, \text{ direct interception parameter}$$

$$N_{Re} = \frac{D_f V_o \rho}{\mu}, \text{ Reynolds number}$$

- β = packing density, fraction of volume of filter occupied by fibers, dimensionless
- ϵ_o = permittivity of free space = $(8.85)(10^{-21})$ coulomb²/dyne cm²
- ϵ_p = dielectric constant of aerosol particle, dimensionless
- ϵ_f = dielectric constant of gas, dimensionless
- η = target efficiency, collection efficiency of isolated filter element, dimensionless
- η_e = effective efficiency of element as functioning in a filter, dimensionless
- λ = mean free path of an air molecule, in feet
- μ = dynamic viscosity of gas, in slugs per foot minute or pounds force per minute per square foot
- ρ = density of gas, in slugs per cubic foot
- ρ_f = density of filter material, in slugs per cubic foot
- ρ_p = density of particle, in slugs per cubic foot
- σ_g = geometric deviation, dimensionless